# PCLAF-DREAM Drives Alveolar Cell Plasticity for Lung Regeneration

Bongjun Kim,[1] Yuanjian Huang,[1] Kyung-Pil Ko,[1] Shengzhe Zhang,[1] Gengyi Zou,[1] Jie Zhang,[1] Moon Jong Kim,[1] Danielle Little,[2] Lisandra Vila Ellis,[2] Margherita Paschini,[3] Sohee Jun,[1] Kwon-Sik Park,[4] Jichao Chen,[2] Carla Kim,[3] Jae-Il Park[1,5,6,*]

[1]Department of Experimental Radiation Oncology, Division of Radiation Oncology, The University of Texas MD Anderson Cancer Center, Houston, TX 77030, USA
[2]Department of Pulmonary Medicine, The University of Texas MD Anderson Cancer Center, Houston, TX 77030, USA
[3]Stem Cell Program and Divisions of Hematology/Oncology and Pulmonary Medicine, Boston Children's Hospital, Boston, MA 02115, USA
[4]Department of Microbiology, Immunology, and Cancer Biology, University of Virginia, Charlottesville, VA 22908, USA
[5]Graduate School of Biomedical Sciences, The University of Texas MD Anderson Cancer Center, Houston, TX 77030, USA
[6]Program in Genetics and Epigenetics, The University of Texas MD Anderson Cancer Center, Houston, TX 77030, USA

*Correspondence: Jae-Il Park
E-mail: jaeil@mdanderson.org; Tel: 713-792-3659; Fax: 713-794-5369
Keywords: PCLAF, PAF, KIAA0101, DREAM complex, cell plasticity, lung regeneration, alveolar cells, phenelzine

## One Sentence Summary

PCLAF-DREAM-driven cell plasticity is essential for lung regeneration, pharmacologically manipulated as a preventive strategy for lung fibrosis.

## Abstract

The spatiotemporal orchestration of stem/progenitor cells is essential for lung regeneration, the failure of which leads to lung disease, including fibrosis. However, the mechanism of alveolar cell plasticity during regeneration remains elusive. We previously found that PCLAF remodels the DREAM complex for cell quiescence exit and cell proliferation. PCLAF is expressed explicitly in pulmonary proliferative cells, along with the DREAM target genes. Pclaf expression and Pclaf-expressing cells were acutely increased upon lung injury. Intriguingly, *Pclaf* knock-out mice exhibited lung fibrosis resulting from alveolar type I (AT1) cell loss. The single-cell transcriptome and organoid analyses showed that Pclaf-DREAM complex–transactivated gene expression is required for alveolar type II (AT2) cell transition into AT1. Mechanistically, Clic4, transactivated by the Pclaf-DREAM complex, activates TGF-β signaling for AT2-PPCs-AT1 cell lineage trajectory. Furthermore, pharmacological mimicking of the Pclaf-mediated transcriptome markedly increased alveolar regeneration. Our study unveils an unexpected role of the PCLAF-DREAM axis in controlling alveolar cell plasticity for lung regeneration and proposes a viable option for lung fibrosis prevention.

## Introduction

Lung disease is one of the leading causes of death, with one in six deaths worldwide (*1*). Various environmental pathogens and stresses cause lung injuries (*2-4*). Stem and progenitor cell–driven regenerative potency functionally restores damaged lungs (*5, 6*). The failure of lung stem/progenitor cell activation or differentiation results in lung disease, including pulmonary fibrosis (*5-8*). Alveolar type II (AT2) cells have been suggested as a pivotal cell type in lung regeneration. Dysregulation of the facultative progenitor capacity of AT2 cells induces lung fibrosis rather than regeneration (*7, 9-13*). Downregulation of Toll-like receptor 4-hyaluronan interaction (*7*) and sustained mechanical tension (*13*) inhibits AT2 cell stemness and plasticity. Telomere dysfunction (*10*) and mutant surfactant protein C (SPC) (*11*) promote AT2 cell hyperplasia, causing the failure of lung regeneration. Therefore, the precise control of AT2 cells is vital for lung regeneration. However, the detailed mechanism of AT2 cell activation and plasticity remains ambiguous.

The dimerization partner, retinoblastoma (RB)-like, E2F, and multi-vulval class B (DREAM) complex is an evolutionarily conserved multiprotein complex that orchestrates cell quiescence and the cell cycle (*14-17*). Dissociation of the multi-vulval class B (MuvB) core complex with RBL2 (retinoblastoma-like protein 2/p130), E2F4, and DP1 (E2F dimerization partner 1) drives the MuvB complex to bind to BYMB and FOXM1, transactivating cell cycle-related DREAM target genes and leading to cell quiescence exit and cell proliferation (*18*). We recently found that proliferating cell nuclear antigen–associated factor (PCLAF/PAF/KIAA0101) remodels the DREAM complex to bypass cell quiescence and promote cell proliferation (*19*). PCLAF is also indispensable for cell stemness and the plasticity of breast cancer cells and intestinal stem cells (*20, 21*). These studies led us to evaluate the role of PCLAF in lung regeneration.

## Results

### PCLAF-positive cells are elevated during lung regeneration

We first characterized PCLAF-positive cells in the lungs by analyzing the data set of single-cell RNA-sequencing (scRNA-seq) of murine (GSE141259) and human (GSE135893) lung tissues. The mouse lungs showed that Mki67$^+$ pulmonary proliferating cells (PPCs) specifically expressed *Pclaf* (Fig. 1, A to C). These PPCs barely expressed mature lung epithelial cell markers or lung stem/progenitor cell markers (Fig. S1, A, C, and D, and Data file S1). The human lungs also showed specific expression of PCLAF in PPCs (Fig. 1, D to F, Fig. S1, B, E, and F, and Data file S2). To understand the role of PCLAF in lung regeneration, we utilized a bleomycin-induced lung injury mouse model, widely used to study lung injury, regeneration, and fibrosis (*22*). Upon the instillation of bleomycin, the number of PPCs was elevated in the mouse lungs (Fig. 1G). Bleomycin injury also led to increased *Pclaf* expression, which peaked at 7 days post-injury (dpi) and decreased at 14 dpi in the mouse lung tissues (Fig. 1H), consistent with the immunostaining results for Pclaf (Fig. 1I). In addition, *Pclaf-lacZ* knock-in mice displayed a similar increase in Pclaf$^+$ cells in the regenerating lungs (Fig. 1, J to L).

## Pclaf is indispensable for repopulation of AT1 cells during lung regeneration

Next, to determine the role of PCLAF in lung regeneration, we administered a low dose of bleomycin (1.4 U/kg) to *Pclaf* wild-type (WT) and knock-out (KO) mice (Fig. 2A). Bleomycin initially damages the alveolar epithelium, including alveolar type I (AT1) and AT2 cells, followed by inflammation and interstitial fibrosis (*22*-*24*). At the early stage of bleomycin administration, both *Pclaf* WT and KO mice exhibited a gradual decrease in blood oxygen levels (peripheral oxygen saturation [$SpO_2$]) and breath rate per minute until 5 dpi (Fig. 2B). Interestingly, *Pclaf* KO mice showed the attenuated and delayed restoration of $SpO_2$ saturation and breath rate per minute at 9 dpi and decreased $O_2$ saturation at 21 dpi (Fig. 2B). At the acutely damaged stage (3 dpi), both *Pclaf* WT and KO mice showed a severely reduced number of $Rage^+$ (AT1) and $Spc^+$ (AT2) cells (Fig. 2, C and D, and Fig. S2). However, consistent with the results of pulmonary functional analysis, *Pclaf* KO showed decreased AT1 cells at the regeneration stage (7 dpi) and chronic fibrosis stage (21 dpi) (Fig. 2, C and D, and Fig. S2). Intriguingly, the number of AT2 cells was elevated in *Pclaf* KO mice upon bleomycin (Fig. 2, C and D, and Fig. S2). Unlike WT lung tissues, *Pclaf* KO lungs exhibited more inflamed and condensed tissue (Fig. 2E), with severe fibrotic features confirmed by picrosirius red (a dye staining collagen) and αSma/Acta2 (a marker for myofibroblasts) staining (Fig. 2, F to H). These results suggest that Pclaf is indispensable for bleomycin-induced lung regeneration.

AT2 cells replenish AT1 cells during lung regeneration (*25*). Having observed that *Pclaf* KO impaired lung regeneration with the aberrantly increased AT2 cells, we next determined the impact of *Pclaf* KO on cell plasticity between AT2 and AT1 cells by using lung organoids (LOs). We evaluated the lung organoid-forming efficiency (OFE) and cellular heterogeneity generation of two different LO culture methods, co-culture systems with lung endothelial cells (LuECs) or lung mesenchymal cells (LuMSCs) in the 3D organoid air-liquid interface (Fig. S3A) (*26*-*28*). Both culture methods were sufficient to grow LOs (Fig. S3A). While LOs with LuMSCs were mainly differentiated into the bronchiolar type, LOs co-cultured with LuECs developed into both alveolar and bronchiolar types of LOs (Fig. S3, B to D), which led us to choose LuECs as stromal cells for subsequent LO experiments. We isolated and cultured lung epithelial cells ($Epcam^+/Ter119^-/Cd31^-/Cd45^-$) from *Pclaf* WT or KO mice at 7 dpi (bleomycin) with LuECs (Fig. 2I). Notably, OFE was reduced in *Pclaf* KO cells compared to in *Pclaf* WT cells (Fig. S4, A and B). In addition, *Pclaf* KO LOs showed fewer alveolar (~12%) and bronchioalveolar types (~50%), whereas *Pclaf* WT LOs displayed alveolar (~27%) and bronchioalveolar types (~70%) (Fig. S4, C and D). Interestingly, the bronchiolar type of LOs was generated only by *Pclaf* KO (~29%) (Fig. S4, C and D). Moreover, *Pclaf* KO alveolar-type LOs showed fewer AT1 cells, consistent with in vivo results (Fig. 2, J and K). These data indicate that Pclaf is required for the plasticity of AT1 and AT2 cell lineage during lung regeneration.

## *Pclaf* KO suppresses AT2 cell lineage plasticity

To further explore the cellular mechanism of Pclaf-controlled lung regeneration, we leveraged single-cell transcriptomics. We isolated pulmonary epithelial cells from *Pclaf* WT or KO lung tissues at 7 dpi (bleomycin) and performed scRNA-seq (Fig. S5A). Cells were clustered and annotated based on the established cell markers (Fig. 3, A and B, Fig. S5B, Fig. S6, and Data file S3). The AT2 cells were refined into two subsets, AT2 ($Lcn2^{high}$) and AT2 ($Slc34a2^{high}$) cells (Fig.

3B, Fig. S6, D and E). Consistent with the in vitro and in vivo results, *Pclaf* KO lungs showed reduced AT1 cells and elevated AT2 (Slc34a2$^{high}$) cells (Fig. 3, B and C). Additionally, AT2$^{med}$/AT1$^{med}$ cells, transitioning cells from AT2 into AT1 (*29, 30*), were decreased in *Pclaf* KO mice (Fig. 3, B and C). In line with previous studies (*25, 29, 30*), an RNA velocity–based cell lineage trajectory analysis showed the cellular trajectory from AT2 cells into AT1 cells in *Pclaf* WT (Fig. 3, D to F, and 3H). AT2 (Lcn2$^{high}$) cells serve as root cells that differentiate into AT1 cells through two different paths, via AT1$^{med}$/AT2$^{med}$ cells or PPCs and Krt8$^{+}$ cells. Additional cell lineage trajectories from AT2 (Lcn2$^{high}$) cells to AT2 (Slc34a2$^{high}$) cells through PPCs were observed (Fig. 3, D to F, and 3H). Unlike *Pclaf* WT, *Pclaf* KO lung showed a favored trajectory of PPCs into AT2 (Slc34a2$^{high}$) cells (Fig. 3, D to F, and 3H). Additionally, in *Pclaf* KO lungs, Krt8$^{+}$ cells and AT1$^{med}$/AT2$^{med}$ cells showed lineage trajectories into AT2 (Lcn2$^{high}$) and AT2 (Slc34a2$^{high}$) cells, respectively, rather than toward AT1 cells (Fig. 3, D to F, and 3H). Consistently, the CytoTRACE analysis showed a less differentiated cell status in transitioning AT1$^{med}$/AT2$^{med}$ cells of *Pclaf* KO lungs than of WT lungs (Fig. 3G). While AT2 cells self-renewed and differentiated into AT1 cells via PPCs for normal lung regeneration, *Pclaf* KO impaired AT1 differentiation from PPCs derived from AT2 cells (Fig. 3H). These results suggest that Pclaf promotes the cell plasticity of AT2 and PPCs into AT1 for lung regeneration.

## PCLAF-DREAM axis is required for AT1 cell differentiation cells during lung regeneration

Next, we sought to elucidate the underlying mechanism of PCLAF-controlled AT2 cell plasticity. PCLAF remodels the repressive DREAM complex to activate the target gene transcription (*19*). Consistent with the specific expression of PCLAF/Pclaf in PPCs, the expression of DREAM target genes was exclusively enriched in the PPCs of human and mouse lung tissues (Fig. 4, A and B, and Fig. S7A), also confirmed by gene set enrichment analysis (GSEA) of *Pclaf* WT vs. KO lung tissues (Fig. 4C, and Fig. S7B). Intriguingly, *Pclaf* KO PPCs displayed lower expression of the DREAM target genes than did *Pclaf* WT PPCs (Fig. 4D), implying that the DREAM complex might be functionally associated with PCLAF-controlled AT2 cell plasticity. To test this, we pharmacologically and genetically manipulated the DREAM complex in the LOs isolated from the mice treated with bleomycin. First, we used harmine, an inhibitor of DYRK1A that suppresses the DREAM complex (*31, 32*). DYRK1A-phosphorylated serine residue (Ser28) of LIN52, a core subunit of the DREAM/MuvB complex, is essential for recruiting RBL2/p130, E2F4, and DP1 to the MuvB core complex to form a repressive DREAM complex, which subsequently suppresses gene transactivation. Thus, harmine-inhibited DYRK1A constitutively activates DREAM target gene expression. Harmine treatment rescued OFE inhibited by *Pclaf* KO (Fig. 4, E to G). Harmine also restored the lung regeneration impaired by *Pclaf* KO, with increased AT1 and decreased AT2 cells (Fig. 4, H and I). Moreover, the ectopic expression of the Lin52-S28A mutant, which is no longer phosphorylated by DYRK2 and consequently activates the DREAM target gene expression, rescued the *Pclaf* KO phenotype by AT1 cell repopulation, restored the number of AT2 cells, and increased OFE (Fig. 4, J to L, and Fig. S8). WNT signaling maintains AT2 cell stemness (*33*). Although PCLAF hyperactivates WNT/β-catenin in the intestine (*21, 34*), β-catenin target genes (*Cd44*, *Ccnd1*, and *Bmp4*) were marginally downregulated in *Pclaf* KO PPCs. Additionally, the Sox9-based progenitor gene signature, which positively regulates lung stem/progenitor cell plasticity (*35*), and *Myc* transactivated by Pclaf in the intestine (*21*) were not downregulated in

*Pclaf* KO PPCs (Fig. S9). These results suggest that the PCLAF-DREAM axis–controlled transcriptome mediates alveolar cell lineage plasticity for lung regeneration.

## PCLAF-DREAM-activated CLIC4-TGFβ signaling axis is required for AT1 cell differentiation

Among the differentially expressed genes (DEGs; *Pclaf* WT vs. KO) of the DREAM target genes, *Clic4* showed reduced expression in transitioning cells (PPC, Krt8$^{+}$, and AT2$^{med}$/AT1$^{med}$ cells (Fig. S10A), validated by immunostaining (Fig. 5, A and B). CLIC4 is an integral component of TGF-β signaling, required to transdifferentiate AT2 cells into AT1 cells during lung regeneration (*36, 37*). CLIC4 positively modulates TGF-β signaling by preventing the dephosphorylation of phospho-SMAD2/3 in the nucleus (*38, 39*). Given the crucial role of TGF-β/SMAD signaling in the lung regeneration (*36, 37*), we hypothesized that the PCLAF-DREAM-activated CLIC4-TGF-β signaling axis is required for AT2 cell plasticity into AT1 cells. Indeed, SMAD3 target genes from three datasets (*40, 41*) were downregulated in *Pclaf* KO PPCs but not in other cell types compared to WT (Fig. 5C). In addition, a GSEA showed the enrichment of Smad2 or Smad3 target gene expression in *Pclaf* WT PPCs compared to in *Pclaf* KO PPCs (Fig. 5D, and Fig. S7B). Moreover, a SCENIC gene network analysis showed reduced Smad3 regulon activity in *Pclaf* KO PPCs and Krt8$^{+}$ cells (Fig. 5E), consistent with the reduced p-Smad3 in the lung of *Pclaf* KO mice treated with bleomycin, compared to the *Pclaf* WT regenerating lung (Fig. 5, F and G). Conversely, harmine treatment restored Clic4 and p-Smad3 expression downregulated by *Pclaf* KO (Fig. S10, B to E). Next, to determine the role of the CLIC4-TGF-β signaling axis in AT2 cell plasticity, we ectopically expressed Clic4 in *Pclaf* KO LOs. Clic4 expression increased phosphorylation of Smad3 (Fig. S10, F and G) and rescued the AT1 differentiation blocked by *Pclaf* KO (Fig. 5, H to J, and Fig. S10H), as did temporarily controlled TGF-β treatment (Fig. 5, K to N, and Fig. S11). Notably, human PPCs from idiopathic pulmonary fibrosis (IPF) showed reduced CLIC4 and SMAD3-target genes expression compared to PPCs from normal lungs (Fig. 5, O and P). TGF-β signaling also contributes to lung fibrosis (*42*). While regenerating alveoli lesions showed decreased p-Smad3 by *Pclaf* KO, the inflamed lesions exhibited elevated p-Smad3 (Fig. S12). Additionally, human IPF fibroblasts showed increased SMAD3-target gene expression compared to normal lung fibroblasts (Fig. S13). These results suggest that the PCLAF-DREAM-activated CLIC4-TGF-β axis is required for AT2 cell plasticity in lung regeneration.

## Pharmacological mimicking of PCLAF-DREAM-activated transcriptional signature attenuates lung fibrosis

For the pharmaceutical application of PCLAF-DREAM-controlled lung regeneration, we exploited the perturbational datasets (L1000) using the CLUE platform (*43*), identifying drug candidates that mimic PCLAF-activated transcriptional signatures. Since PCLAF also promotes lung tumorigenesis (*19*), to minimize the risk of tumorigenesis by drug candidates, we excluded any drugs that were identified from the Pclaf/PCLAF depleted gene sets of the mouse lung tumors (*Kras$^{G12D}$/Trp53$^{-/-}$*; KP) and human (H1792) lung cancer cell lines (Fig. 6, A and B, and Data file S4 and S5) (*19*), which identified four drugs (phenelzine, trimethobenzamide, ibuprofen, and RS 23597-190) (Fig. 6B). Among those, phenelzine, an FDA-approved anti-depressor, increased OFE (Fig. S14) and AT1 cells in LOs (Fig. 6, C and D). Additionally, phenelzine reduced the numbers

of ciliated cells and elevated club cells in LOs (Fig. 6, C and D). Next, we tested the impact of phenelzine on lung regeneration in mice given a high dosage of bleomycin (2.7 U/kg). Phenelzine ameliorated bleomycin-decreased $SpO_2$ levels (Fig. 6F) and markedly reduced lung fibrosis with a restored AT1 cell repopulation (Fig. 6, G to J). These data suggest that phenelzine, a PCLAF activation–mimicking drug, has therapeutic efficacy in lung regeneration and fibrosis.

## Discussion

Accumulating evidence suggests that during alveolar regeneration, AT2 cells act as progenitor cells that differentiate toward AT1 cells through intermediate cell states. Such transient cells express low levels of AT1 and AT2 markers and their specific genes, such as *Krt8 (25, 29, 30)*. Several developmental signaling pathways (BMP (*44*), NOTCH (*44*), and YAP/TAZ (*45*)) contribute to cell transition from AT2 to AT1 during regeneration. However, the detailed mechanism of AT2 cell lineage plasticity during regeneration remains elusive. Our study identified a new role of the PCLAF-DREAM axis in cell plasticity (from AT2 to AT1). The primary function of the DREAM complex in orchestrating the cell cycle and cell quiescence by transactivating or repressing gene expression has mainly been investigated using in vitro systems (*17, 18, 46-51*). Recently, we found that the deregulated DREAM complex promotes lung tumorigenesis in vivo (*19*). Genome-wide analyses showed that most DREAM target genes are cell cycle-related genes (*46, 50*) and genes involved in other biological processes (Data file S6). Given that the DREAM complex coordinates the cell cycle (*17, 18, 46-50*), we initially hypothesized that the PCLAF-DREAM axis induces mitotic activation of lung progenitor cells for regeneration. Indeed, the expression of cell cycle-related genes (*Top2a* and *Mki67*) were decreased in *Pclaf* KO PPCs (Fig. S10A) with reduced OFE (Fig. S4, A and B). However, *Pclaf* KO mice showed a slightly higher number of PPCs than *Pclaf* WT mice (Fig. 3C), which might be due to "stalled" transitioning from PPCs to $Krt8^+$ cells. Unlike *Pclaf* WT PPCs, which show cellular trajectory into AT2 ($Slc34a^{high}$) and $Krt8^+$ cells during normal regeneration, *Pclaf* KO PPCs failed to differentiate into $Krt8^+$ cells (Fig. 3, D to F, and 3H), which might result in an increased number of PPCs in *Pclaf* KO mice. In addition, it should be noted that the number of AT2 ($Slc34a^{high}$) cells differentiated from PPCs was elevated by *Pclaf* KO (Fig. 2 and 3). Intriguingly, our data also showed that DREAM complex–mediated gene transactivation is indispensable for the differentiation of PPCs into AT1 cell lineage (Fig. 4). Clic4 transactivated by the PCLAF-DREAM complex positively modulates TGF-β signaling (*38*), driving PPCs to AT1 differentiation (Fig. 5). Our results unveil an unexpected role of the DREAM complex in positively regulating cell plasticity and promoting tissue regeneration beyond its canonical role in controlling cell quiescence and proliferation.

Despite the recent single-cell transcriptomics of the lungs (*29, 30, 35, 52*), the proliferating cell clusters have not been studied. Herein, our results suggest that PPCs are the transitioning cells during alveolar regeneration. Recently, Murthy et al. proposed that AT0 cells expressing *SFTPC* and *SCGB3A2* transiently differentiate into AT1 cells in human lungs (*53*). These AT0 cells are proliferating cells expressing MKI67 (*53*), consistent with our finding that PPCs are intermediate transitioning cells generating AT1 cells.

TGF-β signaling has been proposed as one of the driving factors for lung fibrosis (*54*) by promoting the epithelial-mesenchymal transition of AT2 cells (*55*). Other studies suggest that TGF-β signaling is required for the alveolar cell plasticity (*36*) and alveolar regeneration (*37*). Our results showed that TGF-β signaling is necessary for AT1 cell regeneration in the context of PPCs. In *Pclaf* KO lung, p-Smad3 was significantly decreased in regenerative alveoli lesions (Fig. 5, F and G) but elevated in inflamed fibrotic lesions (Fig. S12). In line with this, SMAD3-target genes were downregulated in IPF PPCs while upregulated in IPF fibroblasts compared to normal lungs (Fig. 5, O and P, and Fig. S13). Thus, it is highly likely that TGF-β signaling spatiotemporally contributes to lung fibrosis or regeneration, depending on cell types or lesions.

The current therapeutic strategy for lung fibrosis has focused on inhibiting fibroblasts using pirfenidone and nintedanib (*56*). Recent studies suggested that failure of lung regeneration is one of the fundamental pathogeneses of lung fibrosis (*7, 9-13*). Intriguingly, disrupted AT2 cell lineage plasticity by *Pclaf* KO drove lung fibrosis rather than lung regeneration (Fig. 2). Based on our findings, we identified PCLAF-activation–mimicking drugs and validated their therapeutic impact on lung regeneration in vivo and in vitro (Fig. 6). This strategy, which facilitates the repopulation of functional lung epithelial cells, may be an alternative regimen or preventive measure for lung fibrosis caused by thoracic radiotherapy in lung cancer patients.

The *Pclaf* KO mice showed slight alteration of immune cell status (*57*). Since immune cells also play an essential role in lung regeneration and disease (*58*), the impact of *Pclaf* KO on immune cells may contribute to the lung regeneration phenotype. Nonetheless, consistent with the *Pclaf* KO mouse phenotype, the results from lung organoids without immunocytes suggest that the role of the PCLAF-DREAM axis in lung epithelial cell plasticity is independent of immune cells. Although mouse and organoid models have been extensively employed to study lung pathophysiology, our finding in murine systems remains to be tested in a human-relevant system, such as human lung organoids.

Together, our comprehensive approaches reveal a new role of the PCLAF-DREAM axis in driving alveolar cell plasticity via CLIC4-TGF-β for lung regeneration. Furthermore, this study suggests that phenelzine, a drug mimicking the PCLAF-DREAM transcriptional signature, may be a viable therapeutic option for lung disease.

## Acknowledgments

We are grateful to Pierre D. McCrea and Malgorzata Kloc for insightful comments; Joel M. Sederstrom for technical assistance; Stuart H. Yuspa (Center for Cancer Research, NCI) for reagents (pAltermax-3HA-CLIC4); Ann Sutton (Research Medical Library, MD Anderson) for editing the manuscript. This work was supported by the Cancer Prevention and Research Institute of Texas (RP200315 to J.-I.P.), the National Cancer Institute (CA193297 and CA256207 to J.-I.P.), an Institutional Research Grant (MD Anderson to J.-I.P.), Specialized Program of Research Excellence (SPORE) grant in endometrial cancer (P50 CA83639), and Radiation Oncology Research Initiatives. The core facilities at MD Anderson (DNA sequencing and Genetically Engineered Mouse Facility) were supported by National Cancer Institute Cancer Center Support Grant (P30 CA016672 to MD Anderson). The core facilities at Baylor College of Medicine (Cytometry & Cell Sorting Core and Single Cell Genomics Core) were supported by CPRIT (RP180672, RP200504) and the National Institutes of Health (CA125123, RR024574).

## Author contributions

Conceptualization: B.K. and J.-I.P.; Methodology: B.K., L.V.E., K.-S.P., J.C., M.P., C.K., and J.-I.P.; Validation: B.K. and J.-I.P.; Formal analysis: B.K. and J.-I.P.; Investigation: B.K., Y.H., K.-P.K., S.Z., G.Z., J.Z., M.J.K., S.J., and J.-I.P.; Data Curation: B.K., D.L., and J.C.; Visualization: B.K. and J.-I.P.; Supervision: J.-I.P.; Project administration: B.K. and J.-I.P.; Funding acquisition: J.-I.P.; Writing - Original Draft: B.K. and J.-I.P.

**Competing interests:** All authors declare that they have no competing interests.

## Data and material availability

### Data availability

Bulk and scRNA-seq data are available via the Gene Expression Omnibus (GSE205815; https://www.ncbi.nlm.nih.gov/geo/query/acc.cgi?acc=GSE205815).
(Log-in token for reviewers: ____)

### Code availability

The code used to reproduce the analyses described in this manuscript can be accessed via GitHub (https://github.com/jaeilparklab/Pclaf_lung_regeneration) and will also be available upon request.

## Materials and methods

### Mice

All mouse experiments were approved by the MD Anderson Institutional Animal Care and Use Committee and performed under MD Anderson guidelines and the Association for Assessment and Accreditation of Laboratory Animal Care international standards. *Pclaf* KO mice from a previously established model (*21*) were used. The *Pclaf-lacZ* knock-in strain was generated by breeding *Pclaf-lacZ-neo* mice with *Rosa26-Cre* driver mice. The *Pclaf-lacZ-neo* strain was established by in vitro fertilization of the sperm carrying the Pclaf-lacZ-neo targeted allele (C57BL/6N-A$^{tm1Brd}$ Pclaf$^{tm1a(EUCOMM)Wtsi}$/WtsiPh; EMMA ID: EM:09820). The targeted or recombinant alleles were validated by genomic DNA PCR and Sanger sequencing.

### Bleomycin-induced lung injury

Eight to ten-week-old mice were anesthetized via inhalation of isoflurane using a calibrated vaporizer for approximately 3 mins. The mice were positioned on the intratracheal intubation stand and intubated IV catheters (22GA × 1.00 IN, 0.9 × 25 mm; BD, NJ) in the trachea using BioLite (Biotex, TX) intubation system with optic fiber. The intubated mice were given 1.25 U/kg of bleomycin in 50 µl of PBS. One day before the injury, the blood arterial oxygen saturation and breath rate per minute were recorded using a small rodent oximeter sensor mounted on the thigh of each tested mouse (MouseOX; STARR Life Sciences, Oakmont, PA) every other day. Data were collected for a minimum of 10 seconds with no error code. The mice were euthanized at the acute injury phase (3 days after injury [dpi], regeneration phase [7 dpi], and chronic fibrotic phase [21 dpi]) for post-mortem lung tissue collection, followed by histology.

### Histology and immunohistochemistry

Lung tissues were perfused with cold phosphate-buffered saline (PBS, pH 7.4) into the right ventricle, fixed with 10% formalin, embedded in paraffin, and sectioned at 5-µm thickness. The sections were stained with hematoxylin and eosin for histological analysis. For picrosirius red staining, deparaffinized and hydrated sections were stained with picrosirius red solution (0.1% Direct Red 80 [Sigma] in saturated [1.3%] picric acid) for 1 hr. Sections were washed with 0.5% acetic acid and dehydrated before mounting. For the immunohistochemistry analysis, sections were immunostained according to standard protocols(*19*). For antigen retrieval, sections were subjected to heat-induced epitope retrieval pre-treatment at 120 °C using citrate-based antigen unmasking solution (Vector Laboratories, Burlingame, CA, USA), tris-based antigen unmasking solution (Vector Laboratories), or universal antigen retrieval reagent (R&D System). Specific information on antibodies is described in Data file S7.

### X-gal staining

Lung tissues were perfused with cold phosphate-buffered saline (PBS, pH 7.4) into the right ventricle, incubated with a mixture of 30% sucrose and 10% optimal cutting temperature (OCT) compound in PBS for 30min at 4 °C, embedded in OCT compound, and sectioned at 10-µm thickness. Frozen lung sections were fixed with 0.2% glutaraldehyde for 10 mins and washed in wash buffer (0.02% IGEPAL CA-630, 0.01% sodium deoxycholate, 2mM $MgCl_2$, 0.1M phosphate buffer pH 7.5) for 10 mins twice. And then slides were incubated with X-gal staining solution (1 mg/ml X-gal, 5mM potassium ferricyanide, 5mM potassium ferrocyanide in wash buffer) for 16 hours in 37 °C. X-gal-stained slides were post-fixed with 4% PFA for 10 min and washed with

PBS for 5 mins 3 times. For counterstaining, slides were incubated with nuclear fast red solution (Vector Laboratories, Burlingame, CA, USA) for 2 mins.

**Lung cell isolation**

Lungs were harvested from euthanized mice after perfusing 10 ml of cold PBS into the right ventricle. Lungs were minced after the removal of extra-pulmonary tissues and digested in Leibovitz media (Gibco, USA, no. 21083-027) with 2 mg/ml collagenase type I (Worthington, CLS-1, LS004197), 2 mg/ml elastase (Worthington, ESL, LS002294), and 0.4 mg/ml DNase I (Sigma, DN-25) for 45 min at 37 °C. To stop the digestion, fetal bovine serum (FBS, HyClone; Cytiva) was added to a final concentration of 20%. The digested tissues were sequentially filtered through a 70-μm and a 40-μm cell strainer (Falcon, 352350 and 352340, respectively). The samples were incubated with 1 ml of red blood cell lysis buffer (15 mM $NH_4Cl$, 12 mM $NaHCO_3$, 0.1 mM EDTA, pH 8.0) for 2 min on ice. Leibovitz with 10% FBS and 1 mM EDTA was used for resuspension and washing for magnetic-activated cell sorting (MACS) or fluorescence-activated cell sorting.

For lung epithelial cell isolation, cells were resuspended in 400 μl of buffer with 30 μl of CD31 MicroBeads (130-097-418; Miltenyi Biotec, Bergisch Gladbach, Germany), 30 μl of CD45 MicroBeads (130-052-301; Miltenyi Biotec), and 30 μl of anti-Ter-119 MicroBeads (130-049-901; Miltenyi Biotec) and incubated for 30 min at 4 °C, followed by negative selection according to the manufacturer's instructions. Cells were then resuspended with 400 μl of buffer with 30 μl of CD326 (EpCAM) MicroBeads (130-105-958; Miltenyi Biotec) and incubated for 30 min at 4 °C, followed by positive selection according to the manufacturer's instructions. Isolated lung epithelial cells were used for the lung organoid culture. In single-cell RNA sequencing (scRNA-seq), digested lung cells were resuspended in 400 μl of buffer with 5 μl of anti-CD31-FITC (BD Biosciences, CA, USA), 5 μl of anti-CD45-APC (BD Biosciences), and 5 μl of anti-CD326 (EpCAM)-PE-Cy7 (BD Biosciences) and incubated for 30 min at 4 °C. Cells were then washed twice, followed by sorting of the epithelial cells by fluorescence-activated cell sorting.

For lung endothelial cell (LuEC) isolation, cells were resuspended in 400 μl of buffer with 30 μl of CD31 MicroBeads and incubated for 30 min at 4 °C, followed by positive selection according to the manufacturer's instructions. Isolated LuECs were cultured with EC growth media (DMEM; Corning; 10-013-CV, 20% FBS, 1× glu-pen-strep; Gibco, USA; 10378016, 100 μg/ml endothelial cell growth factor (ECGS); Sigma; E2759, 100 μg/ml heparin; Sigma; H3149, 25 mM HEPES) on 0.1% gelatin (Sigma, G1393)-coated plates. Cultured LuECs were then isolated with CD31 MicroBeads and expanded until passage 3. Expanded LuECs were cryopreserved for lung organoid culture.

**Lung organoid culture**

Lung epithelial cells ($Ter119^-/Cd31^-/Cd45^-/Epcam^+$) isolated from 7-10-week-old *Pclaf* WT or *Pclaf* KO mice at 7 dpi of bleomycin were cultured with lung stromal cells in a 3D organoid air-liquid interface, as described previously(*26-28*). In brief, freshly sorted lung epithelial cells were resuspended in 3D organoid media Dulbecco's modified Eagle's medium (DMEM)/F12 (Gibco, USA), 10% fetal bovine serum (FBS; HyClone, USA), 1× penicillin-streptomycin-glutamine (Gibco, USA), and 1X insulin-transferrin-selenium (Sigma)) and mixed with LuECs at a ratio of 1:1. Cells containing 3D media were mixed with growth factor-reduced Matrigel (BD Biosciences) at a ratio of 1:1. The 100 μl of mixtures containing lung epithelial cells ($5 \times 10^3$) and LuECs ($5 \times 10^4$) were placed in the transwell insert (0.4-μm pore, Corning, Lowell, MA). After incubation for

30 mins at 37°C in an incubator, 500 µl of 3D media were placed in the bottom chamber to generate the liquid-air interface. Media were exchanged every other day, with or without harmine (200 nM; Abcam), phenelzine (10 µM; Cayman, MI, USA), or TGF-β1 (2 ng/ml; R&D System). For viral transduction, freshly isolated lung epithelial cells were resuspended in 500 µl of 3D media containing lentivirus ($2.5 \times 10^7$ TU/ml) and polybrene (7 µg/ml) and centrifuged for 1 hr at 600 g at 32°C. Cells were incubated at 37°C in an incubator for 7 hours, followed by organoid culture.

**Gene construct**

pLenti-CMV-MSC-RFP-SV-Puro vector was purchased from Addgene (#109377) and used as a control vector or backbone for further cloning. For constructing the pLenti-3HA-Clic4-T2A-GFP plasmid, we prepared a pLenti vector backbone using restriction enzymes, XbaI (NEB, USA) and BamHI (NEB, USA). Three DNA fragments of Kozak-3HA, Clic4, and T2A-GFP were amplified with Phusion High-Fidelity DNA Polymerase (NEB, USA) using pLJC5-Tmem192-3HA (Addgene, #102930) for Kozak-3HA, pAltermax-3HA-Clic4(*39*) for Clic4, and pLenti-CMV-mCherry-T2A-GFP for T2A-GFP. We assembled the pLenti-3HA-Clic4-T2A-GFP vector with pLenti backbone and fragments using NEBuilder HiFi DNA Assembly Master Mix (NEB, USA) according to the manufacturer's instructions. Primer information is described in Supplementary Table 7. We used pLenti-3FLAG -Lin52 (WT or S28A), as previously generated (*19*).

**Lentivirus preparation**

Lentiviruses were produced using 2nd-generation packaging vectors in 293T cells. 293T cells were cultured until 70%-80% confluent, and the media were replaced with antibiotics-free DMEM (10% FBS). After 1 hr of media exchange, cells were transfected with vector mixtures in Opti-MEM (Gibco, USA). To generate a vector mixture, pMD2.G (1.3 pmol), psPAX2 (0.72 pmol), DNA (1.64 pmol), and polyethyleneimine (PEI, 39 µg) were added to 800 µl of Opti-MEM and incubated for 15 mins. After 12 hrs of transfection, the media were exchanged with complete media (DMEM, 10% FBS, and 1X penicillin-streptomycin). The virus supernatant was collected after 24 hrs and 48 hrs and filtered with a 0.45-µm syringe filter (Thermo Fisher, CA, USA); polyethylene glycol (PEG) solution (40% PEG-8000 [Thermo Fisher, CA, USA], and 1.2 M NaCl in pH 7.4 PBS) were added in a 3:1 ratio. After overnight incubation of the virus-PEG mixture at 4°C, the virus pellet was generated by centrifugation at 1600X g and 4 °C for 1 hr. The pellet was reconstituted in 1 ml of 3D media and incubated for 15 mins at 4 °C. Reconstituted virus was centrifuged at 20,000X g and 4 °C for 3 mins to remove protein debris. The collected virus was stored in a -80 °C freezer. pLenti-RFP, pLenti-3FLAG-Lin52WT, pLenti-3FLAG -Lin52S28A, and pLenti-3HA-Clic4-T2A-GFP vectors were used for lentivirus generation. For virus titration, $5 \times 10^5$ 293T cells were seeded into 48-well plates (Thermo Fisher, CA, USA). After 24 hrs, cells were infected by the serially diluted virus with 10 µg/ml polybrene. After 48 hrs of transfection, virus transduction units per ml (TU/ml) were measured by fluorescence microscopy.

**Single-cell gene expression library**

Freshly isolated lung epithelial cells from *Pclaf* WT and *Pclaf* KO mice at 7 dpi of bleomycin instillation were used to prepare the single-cell RNA library. To generate single-cell gene expression libraries, $1.6 \times 10^4$ cells per group of single cells were subjected to the Chromium Single Cell Gene Expression 3v3.1 kit (10X genomics) at the Single Cell Genomics Core at Baylor College of Medicine. In brief, reverse transcription (RT) reagents, gel beads containing barcoded

oligonucleotides, and oil were loaded on a chromium controller (×10 Genomics) to generate single-cell gel beads-in-emulsions (GEMs) in which full-length cDNA was synthesized and barcoded for each single-cell. Subsequently, the GEMs were broken, and cDNA from every single cell was pooled. Following clean-up using Dynabeads MyOne Silane Beads, cDNA was amplified by PCR. The amplified product is fragmented to an optimal size before end-repair, A-tailing, and adaptor ligation. The final library was generated by amplification.

**Single-cell RNA sequencing**

Libraries were run on Novaseq for Illumina PE150 sequencing with 20,000 reads per cell. Post-processing and quality control were performed by Novogene using the 10× Cell Ranger package (v. 3.1.0, 10X Genomics). Reads were aligned to the GRCm38 reference assembly using STAR aligner (*59*) (v. 2.7.10a).

**Single-cell RNA preprocessing and quality control**

The Cell Ranger output was used as the input to Seurat v. 4.1.0 for further analysis of the scRNA-seq samples. For each sample, poor-quality cells were filtered based on the number of features (min.features = 200, min.cells = 3), number of RNAs detected (> 200 and < 5000), and percentage of reads arising from the mitochondrial genome (< 20%). We combined *Pclaf* WT and *Pclaf* KO samples using the merge function of Seurat. Clustering using default parameters and uniform manifold approximation and projection (UMAP) non-linear dimensionality reduction were performed using Seurat v. 4.1.0, and we referred to the result as our integrated clusters. The marker genes of each cluster (differentially expressed genes [DEGs] in each cluster compared with all other clusters) and differentially expressed genes between samples were identified with Seurat using the "FindAllMarkers" function with the parameters logfc.threshold = 0.25 and min.pct = 0.25. For the lung epithelial cell analysis, we downsized the *Pclaf* KO sample by one-sixth (from 10,807 cells to 1,797 cells).

**Gene set enrichment analysis**

The DEGs between *Pclaf* WT vs. *Pclaf* KO in the PPC clusters were identified by the Wilcoxon sum test and AUROC statistics using the Presto package v. 1.0.0. They were then subjected to a gene set enrichment analysis (GSEA) using the fgsea package v. 1.16.0. The curated gene sets (C2) in the Molecular Signature Database (MsigDB) v. 7.5.1 were used for the GSEA using the msigdbr package.

**Pseudotime trajectory analysis**

Velocyto.py was used to estimate the RNA velocities of single cells by distinguishing between unspliced and spliced mRNAs in the standard single-cell RNA-sequencing data (*60*). The BAM files, output from Cell Ranger, were subjected to generate loom files containing three categories: "spliced", "unspliced", and "ambiguous". The loom files were applied to calculate the dynamic velocity graph using scVelo v. 0.2.4 (*61*).

**Developmental state analysis**

CytoTRACE v. 0.3.3 was used to predict the relative differentiation state of a single cell (*62*). The cells were given a CytoTRACE score according to their differentiation potential, with a higher score indicating higher stemness/fewer differential characteristics.

**Gene regulatory network analysis**

For regulon identification, a gene regulatory network analysis was performed using the python version of the SCENIC (pySCENIC) method (v. 0.11.2)[63]. pySCENIC integrates a random forest classifier (GENIE3) (v. 1.0.0) to identify potential TF targets based on their co-expression with RcisTarget (v. 0.99.0) for *cis*-regulatory motif enrichment analysis in the promoter of target genes (±500 bp of the transcription start site) and identify the regulon, which consists of a TF and its co-expressed target genes. The *Mus musculus* 10 (mm10) motif database provided by the pySCENIC authors was used. Finally, for each regulon, pySCENIC uses the AUCell (v. 0.99.5) algorithm to score the regulon activity in each cell (Z score, a standardized AUCell score, was used). All parameters used for running were specified in the original pySCENIC pipeline. The ranking databases used were mm10-refseq-r80-10 kb-up-and-down-tss.mc9nr.feather mm10-refseq-r80-500bp-up-and-100bp-down-tss.mc9nr.feather, which were downloaded from https://resources.aertslab.org/cistarget/. The motif database was downloaded from https://resources.aertslab.org/cistarget/motif2tf/.

**Public scRNA-seq data analysis**

A public scRNA-seq data set (GSE141259)(*30*), generated by subjecting sorted cells from the mouse lung epithelial compartment at 18 different time points after bleomycin instillation, was analyzed according to the code provided in the original study. A public scRNA-seq data set (GSE135893)(*52*) was generated from the cells of 20 pulmonary fibrosis and 10 control human lungs and analyzed according to the code provided in the original study.

**Gene expression analysis by qRT-PCR**

RNAs were extracted by TRIzol (Invitrogen) and used to synthesize cDNAs using the iScript cDNA synthesis kit (Biorad). qRT-PCR was performed using an Applied Biosystems 7500 Real-Time PCR machine with the primers listed in Supplementary Table 7. Target gene expression was normalized to that of mouse *Hprt1*. Comparative $2^{-\Delta\Delta Ct}$ methods were used to quantify qRT-PCR results.

## References


1. H. B. Schiller, D. T. Montoro, L. M. Simon, E. L. Rawlins, K. B. Meyer, M. Strunz, F. A. Vieira Braga, W. Timens, G. H. Koppelman, G. R. S. Budinger, J. K. Burgess, A. Waghray, M. van den Berge, F. J. Theis, A. Regev, N. Kaminski, J. Rajagopal, S. A. Teichmann, A. V. Misharin, M. C. Nawijn, The Human Lung Cell Atlas: A High-Resolution Reference Map of the Human Lung in Health and Disease. *Am J Respir Cell Mol Biol* **61**, 31-41 (2019).
2. M. N. Chonghaile, B. D. Higgins, J. Costello, J. G. Laffey, Hypercapnic acidosis attenuates lung injury induced by established bacterial pneumonia. *Anesthesiology* **109**, 837-848 (2008).
3. R. Kc, S. D. Shukla, S. S. Gautam, P. M. Hansbro, R. F. O'Toole, The role of environmental exposure to non-cigarette smoke in lung disease. *Clin Transl Med* **7**, 39 (2018).
4. G. Raghu, H. R. Collard, J. J. Egan, F. J. Martinez, J. Behr, K. K. Brown, T. V. Colby, J. F. Cordier, K. R. Flaherty, J. A. Lasky, D. A. Lynch, J. H. Ryu, J. J. Swigris, A. U. Wells, J. Ancochea, D. Bouros, C. Carvalho, U. Costabel, M. Ebina, D. M. Hansell, T. Johkoh, D. S. Kim, T. E. King, Jr., Y. Kondoh, J. Myers, N. L. Müller, A. G. Nicholson, L. Richeldi, M. Selman, R. F. Dudden, B. S. Griss, S. L. Protzko, H. J. Schünemann, An official ATS/ERS/JRS/ALAT statement: idiopathic pulmonary fibrosis: evidence-based guidelines for diagnosis and management. *Am J Respir Crit Care Med* **183**, 788-824 (2011).
5. D. N. Kotton, E. E. Morrisey, Lung regeneration: mechanisms, applications and emerging stem cell populations. *Nat Med* **20**, 822-832 (2014).
6. M. C. Melo-Narváez, J. Stegmayr, D. E. Wagner, M. Lehmann, Lung regeneration: implications of the diseased niche and ageing. *Eur Respir Rev* **29**, (2020).
7. J. Liang, Y. Zhang, T. Xie, N. Liu, H. Chen, Y. Geng, A. Kurkciyan, J. M. Mena, B. R. Stripp, D. Jiang, P. W. Noble, Hyaluronan and TLR4 promote surfactant-protein-C-positive alveolar progenitor cell renewal and prevent severe pulmonary fibrosis in mice. *Nature Medicine* **22**, 1285-1293 (2016).
8. Y. Kobayashi, A. Tata, A. Konkimalla, H. Katsura, R. F. Lee, J. Ou, N. E. Banovich, J. A. Kropski, P. R. Tata, Persistence of a regeneration-associated, transitional alveolar epithelial cell state in pulmonary fibrosis. *Nature Cell Biology* **22**, 934-946 (2020).
9. J. Katzen, B. D. Wagner, A. Venosa, M. Kopp, Y. Tomer, S. J. Russo, A. C. Headen, M. C. Basil, J. M. Stark, S. Mulugeta, R. R. Deterding, M. F. Beers, An SFTPC BRICHOS mutant links epithelial ER stress and spontaneous lung fibrosis. *JCI Insight* **4**, (2019).
10. R. P. Naikawadi, S. Disayabutr, B. Mallavia, M. L. Donne, G. Green, J. L. La, J. R. Rock, M. R. Looney, P. J. Wolters, Telomere dysfunction in alveolar epithelial cells causes lung remodeling and fibrosis. *JCI Insight* **1**, e86704 (2016).
11. S. I. Nureki, Y. Tomer, A. Venosa, J. Katzen, S. J. Russo, S. Jamil, M. Barrett, V. Nguyen, M. Kopp, S. Mulugeta, M. F. Beers, Expression of mutant Sftpc in murine alveolar epithelia drives spontaneous lung fibrosis. *J Clin Invest* **128**, 4008-4024 (2018).
12. P. A. Reyfman, J. M. Walter, N. Joshi, K. R. Anekalla, A. C. McQuattie-Pimentel, S. Chiu, R. Fernandez, M. Akbarpour, C. I. Chen, Z. Ren, R. Verma, H. Abdala-Valencia, K. Nam, M. Chi, S. Han, F. J. Gonzalez-Gonzalez, S. Soberanes, S. Watanabe, K. J. N. Williams, A. S. Flozak, T. T. Nicholson, V. K. Morgan, D. R. Winter, M. Hinchcliff, C.

L. Hrusch, R. D. Guzy, C. A. Bonham, A. I. Sperling, R. Bag, R. B. Hamanaka, G. M. Mutlu, A. V. Yeldandi, S. A. Marshall, A. Shilatifard, L. A. N. Amaral, H. Perlman, J. I. Sznajder, A. C. Argento, C. T. Gillespie, J. Dematte, M. Jain, B. D. Singer, K. M. Ridge, A. P. Lam, A. Bharat, S. M. Bhorade, C. J. Gottardi, G. R. S. Budinger, A. V. Misharin, Single-Cell Transcriptomic Analysis of Human Lung Provides Insights into the Pathobiology of Pulmonary Fibrosis. *Am J Respir Crit Care Med* **199**, 1517-1536 (2019).

13. H. Wu, Y. Yu, H. Huang, Y. Hu, S. Fu, Z. Wang, M. Shi, X. Zhao, J. Yuan, J. Li, X. Yang, E. Bin, D. Wei, H. Zhang, J. Zhang, C. Yang, T. Cai, H. Dai, J. Chen, N. Tang, Progressive pulmonary fibrosis is caused by elevated mechanical tension on alveolar stem cells. *Cell* **184**, 845-846 (2021).
14. M. M. Harrison, C. J. Ceol, X. W. Lu, H. R. Horvitz, Some C. elegans class B synthetic multivulva proteins encode a conserved LIN-35 Rb-containing complex distinct from a NuRD-like complex. *Proc. Natl. Acad. Sci. U. S. A.* **103**, 16782-16787 (2006).
15. M. Korenjak, B. Taylor-Harding, U. K. Binne, J. S. Satterlee, O. Stevaux, R. Aasland, H. White-Cooper, N. Dyson, A. Brehm, Native E2F/RBF complexes contain Myb-interacting proteins and repress transcription of developmentally controlled E2F target genes. *Cell* **119**, 181-193 (2004).
16. P. W. Lewis, E. L. Beall, T. C. Fleischer, D. Georlette, A. J. Link, M. R. Botchan, Identification of a Drosophila Myb-E2F2/RBF transcriptional repressor complex. *Genes Dev.* **18**, 2929-2940 (2004).
17. L. Litovchick, S. Sadasivam, L. Florens, X. P. Zhu, S. K. Swanson, S. Velmurugan, R. S. Chen, M. P. Washburn, X. S. Liu, J. A. DeCaprio, Evolutionarily conserved multisubunit RBL2/p130 and E2F4 protein complex represses human cell cycle-dependent genes in quiescence. *Mol. Cell* **26**, 539-551 (2007).
18. S. Sadasivam, S. H. Duan, J. A. DeCaprio, The MuvB complex sequentially recruits B-Myb and FoxM1 to promote mitotic gene expression. *Genes Dev.* **26**, 474-489 (2012).
19. M. J. Kim, C. Cervantes, Y. S. Jung, X. Zhang, J. Zhang, S. H. Lee, S. Jun, L. Litovchick, W. Wang, J. Chen, B. Fang, J. I. Park, PAF remodels the DREAM complex to bypass cell quiescence and promote lung tumorigenesis. *Mol Cell* **81**, 1698-1714.e1696 (2021).
20. X. Wang, Y. S. Jung, S. Jun, S. Lee, W. Q. Wang, A. Schneider, Y. S. Oh, S. H. Lin, B. J. Park, J. J. Chen, K. Keyomarsi, J. I. Park, PAF-Wnt signaling-induced cell plasticity is required for maintenance of breast cancer cell stemness. *Nat. Commun.* **7**, 13 (2016).
21. M. J. Kim, B. Xia, H. N. Suh, S. H. Lee, S. Jun, E. M. Lien, J. Zhang, K. F. Chen, J. I. Park, PAF-Myc-Controlled Cell Stemness Is Required for Intestinal Regeneration and Tumorigenesis. *Dev. Cell* **44**, 582-+ (2018).
22. A. Moeller, K. Ask, D. Warburton, J. Gauldie, M. Kolb, The bleomycin animal model: a useful tool to investigate treatment options for idiopathic pulmonary fibrosis? *Int J Biochem Cell Biol* **40**, 362-382 (2008).
23. Y. Kobayashi, A. Tata, A. Konkimalla, H. Katsura, R. F. Lee, J. Ou, N. E. Banovich, J. A. Kropski, P. R. Tata, Persistence of a regeneration-associated, transitional alveolar epithelial cell state in pulmonary fibrosis. *Nat Cell Biol* **22**, 934-946 (2020).
24. T. Sun, Z. Huang, H. Zhang, C. Posner, G. Jia, T. R. Ramalingam, M. Xu, H. Brightbill, J. G. Egen, A. Dey, J. R. Arron, TAZ is required for lung alveolar epithelial cell differentiation after injury. *JCI Insight* **5**, (2019).

25. C. E. Barkauskas, M. J. Cronce, C. R. Rackley, E. J. Bowie, D. R. Keene, B. R. Stripp, S. H. Randell, P. W. Noble, B. L. Hogan, Type 2 alveolar cells are stem cells in adult lung. *J Clin Invest* **123**, 3025-3036 (2013).
26. J. H. Lee, D. H. Bhang, A. Beede, T. L. Huang, B. R. Stripp, K. D. Bloch, A. J. Wagers, Y. H. Tseng, S. Ryeom, C. F. Kim, Lung stem cell differentiation in mice directed by endothelial cells via a BMP4-NFATc1-thrombospondin-1 axis. *Cell* **156**, 440-455 (2014).
27. A. F. M. Dost, A. L. Moye, M. Vedaie, L. M. Tran, E. Fung, D. Heinze, C. Villacorta-Martin, J. Huang, R. Hekman, J. H. Kwan, B. C. Blum, S. M. Louie, S. P. Rowbotham, J. Sainz de Aja, M. E. Piper, P. J. Bhetariya, R. T. Bronson, A. Emili, G. Mostoslavsky, G. A. Fishbein, W. D. Wallace, K. Krysan, S. M. Dubinett, J. Yanagawa, D. N. Kotton, C. F. Kim, Organoids Model Transcriptional Hallmarks of Oncogenic KRAS Activation in Lung Epithelial Progenitor Cells. *Cell Stem Cell* **27**, 663-678.e668 (2020).
28. K. T. Leeman, P. Pessina, J. H. Lee, C. F. Kim, Mesenchymal Stem Cells Increase Alveolar Differentiation in Lung Progenitor Organoid Cultures. *Sci Rep* **9**, 6479 (2019).
29. J. Choi, J. E. Park, G. Tsagkogeorga, M. Yanagita, B. K. Koo, N. Han, J. H. Lee, Inflammatory Signals Induce AT2 Cell-Derived Damage-Associated Transient Progenitors that Mediate Alveolar Regeneration. *Cell Stem Cell* **27**, 366-382.e367 (2020).
30. M. Strunz, L. M. Simon, M. Ansari, J. J. Kathiriya, I. Angelidis, C. H. Mayr, G. Tsidiridis, M. Lange, L. F. Mattner, M. Yee, P. Ogar, A. Sengupta, I. Kukhtevich, R. Schneider, Z. Zhao, C. Voss, T. Stoeger, J. H. L. Neumann, A. Hilgendorff, J. Behr, M. O'Reilly, M. Lehmann, G. Burgstaller, M. Königshoff, H. A. Chapman, F. J. Theis, H. B. Schiller, Alveolar regeneration through a Krt8+ transitional stem cell state that persists in human lung fibrosis. *Nat Commun* **11**, 3559 (2020).
31. N. Göckler, G. Jofre, C. Papadopoulos, U. Soppa, F. J. Tejedor, W. Becker, Harmine specifically inhibits protein kinase DYRK1A and interferes with neurite formation. *Febs j* **276**, 6324-6337 (2009).
32. C. Forristal, S. A. Henley, J. I. MacDonald, J. R. Bush, C. Ort, D. T. Passos, S. Talluri, C. A. Ishak, M. J. Thwaites, C. J. Norley, L. Litovchick, J. A. DeCaprio, G. DiMattia, D. W. Holdsworth, F. Beier, F. A. Dick, Loss of the mammalian DREAM complex deregulates chondrocyte proliferation. *Mol Cell Biol* **34**, 2221-2234 (2014).
33. A. N. Nabhan, D. G. Brownfield, P. B. Harbury, M. A. Krasnow, T. J. Desai, Single-cell Wnt signaling niches maintain stemness of alveolar type 2 cells. *Science* **359**, 1118-1123 (2018).
34. H. Y. Jung, S. Jun, M. Lee, H. C. Kim, X. Wang, H. Ji, P. D. McCrea, J. I. Park, PAF and EZH2 Induce Wnt/beta-Catenin Signaling Hyperactivation. *Mol. Cell* **52**, 193-205 (2013).
35. J. J. Kathiriya, A. N. Brumwell, J. R. Jackson, X. Tang, H. A. Chapman, Distinct Airway Epithelial Stem Cells Hide among Club Cells but Mobilize to Promote Alveolar Regeneration. *Cell Stem Cell* **26**, 346-358.e344 (2020).
36. L. Zhao, M. Yee, M. A. O'Reilly, Transdifferentiation of alveolar epithelial type II to type I cells is controlled by opposing TGF-β and BMP signaling. *Am J Physiol Lung Cell Mol Physiol* **305**, L409-418 (2013).
37. K. A. Riemondy, N. L. Jansing, P. Jiang, E. F. Redente, A. E. Gillen, R. Fu, A. J. Miller, J. R. Spence, A. N. Gerber, J. R. Hesselberth, R. L. Zemans, Single cell RNA sequencing identifies TGFβ as a key regenerative cue following LPS-induced lung injury. *JCI Insight* **5**, (2019).

38. A. Shukla, M. Malik, C. Cataisson, Y. Ho, T. Friesen, K. S. Suh, S. H. Yuspa, TGF-beta signalling is regulated by Schnurri-2-dependent nuclear translocation of CLIC4 and consequent stabilization of phospho-Smad2 and 3. *Nat Cell Biol* **11**, 777-784 (2009).
39. A. Shukla, S. H. Yuspa, CLIC4 and Schnurri-2: a dynamic duo in TGF-beta signaling with broader implications in cellular homeostasis and disease. *Nucleus* **1**, 144-149 (2010).
40. Y. Zhang, D. Handley, T. Kaplan, H. Yu, A. S. Bais, T. Richards, K. V. Pandit, Q. Zeng, P. V. Benos, N. Friedman, O. Eickelberg, N. Kaminski, High throughput determination of TGFβ1/SMAD3 targets in A549 lung epithelial cells. *PLoS One* **6**, e20319 (2011).
41. A. C. Mullen, D. A. Orlando, J. J. Newman, J. Lovén, R. M. Kumar, S. Bilodeau, J. Reddy, M. G. Guenther, R. P. DeKoter, R. A. Young, Master transcription factors determine cell-type-specific responses to TGF-β signaling. *Cell* **147**, 565-576 (2011).
42. U. Bartram, C. P. Speer, The role of transforming growth factor beta in lung development and disease. *Chest* **125**, 754-765 (2004).
43. A. Subramanian, R. Narayan, S. M. Corsello, D. D. Peck, T. E. Natoli, X. Lu, J. Gould, J. F. Davis, A. A. Tubelli, J. K. Asiedu, D. L. Lahr, J. E. Hirschman, Z. Liu, M. Donahue, B. Julian, M. Khan, D. Wadden, I. C. Smith, D. Lam, A. Liberzon, C. Toder, M. Bagul, M. Orzechowski, O. M. Enache, F. Piccioni, S. A. Johnson, N. J. Lyons, A. H. Berger, A. F. Shamji, A. N. Brooks, A. Vrcic, C. Flynn, J. Rosains, D. Y. Takeda, R. Hu, D. Davison, J. Lamb, K. Ardlie, L. Hogstrom, P. Greenside, N. S. Gray, P. A. Clemons, S. Silver, X. Wu, W. N. Zhao, W. Read-Button, X. Wu, S. J. Haggarty, L. V. Ronco, J. S. Boehm, S. L. Schreiber, J. G. Doench, J. A. Bittker, D. E. Root, B. Wong, T. R. Golub, A Next Generation Connectivity Map: L1000 Platform and the First 1,000,000 Profiles. *Cell* **171**, 1437-1452.e1417 (2017).
44. M. I. Chung, M. Bujnis, C. E. Barkauskas, Y. Kobayashi, B. L. M. Hogan, Niche-mediated BMP/SMAD signaling regulates lung alveolar stem cell proliferation and differentiation. *Development* **145**, (2018).
45. R. LaCanna, D. Liccardo, P. Zhang, L. Tragesser, Y. Wang, T. Cao, H. A. Chapman, E. E. Morrisey, H. Shen, W. J. Koch, B. Kosmider, M. R. Wolfson, Y. Tian, Yap/Taz regulate alveolar regeneration and resolution of lung inflammation. *J Clin Invest* **129**, 2107-2122 (2019).
46. S. Sadasivam, J. A. DeCaprio, The DREAM complex: master coordinator of cell cycle-dependent gene expression. *Nat. Rev. Cancer* **13**, 585-595 (2013).
47. N. N. Rashid, R. Yusof, R. J. Watson, Disruption of repressive p130-DREAM complexes by human papillomavirus 16 E6/E7 oncoproteins is required for cell-cycle progression in cervical cancer cells. *J. Gen. Virol.* **92**, 2620-2627 (2011).
48. L. Litovchick, L. A. Florens, S. K. Swanson, M. P. Washburn, J. A. DeCaprio, DYRK1A protein kinase promotes quiescence and senescence through DREAM complex assembly. *Genes Dev.* **25**, 801-813 (2011).
49. M. L. Beshiri, K. B. Holmes, W. F. Richter, S. Hess, A. Islam, Q. Yan, L. Plante, L. Litovchick, N. Gevry, N. Lopez-Bigas, W. G. Kaelin, E. V. Benevolenskaya, Coordinated repression of cell cycle genes by KDM5A and E2F4 during differentiation. *Proc. Natl. Acad. Sci. U. S. A.* **109**, 18499-18504 (2012).
50. M. Fischer, P. Grossmann, M. Padi, J. A. DeCaprio, Integration of TP53, DREAM, MMB-FOXM1 and RB-E2F target gene analyses identifies cell cycle gene regulatory networks. *Nucleic Acids Res.* **44**, 6070-6086 (2016).

51. H. Walston, A. N. Iness, L. Litovchick, DREAM On: Cell Cycle Control in Development and Disease. *Annu Rev Genet* **55**, 309-329 (2021).
52. A. C. Habermann, A. J. Gutierrez, L. T. Bui, S. L. Yahn, N. I. Winters, C. L. Calvi, L. Peter, M. I. Chung, C. J. Taylor, C. Jetter, L. Raju, J. Roberson, G. Ding, L. Wood, J. M. S. Sucre, B. W. Richmond, A. P. Serezani, W. J. McDonnell, S. B. Mallal, M. J. Bacchetta, J. E. Loyd, C. M. Shaver, L. B. Ware, R. Bremner, R. Walia, T. S. Blackwell, N. E. Banovich, J. A. Kropski, Single-cell RNA sequencing reveals profibrotic roles of distinct epithelial and mesenchymal lineages in pulmonary fibrosis. *Sci Adv* **6**, eaba1972 (2020).
53. P. Kadur Lakshminarasimha Murthy, V. Sontake, A. Tata, Y. Kobayashi, L. Macadlo, K. Okuda, A. S. Conchola, S. Nakano, S. Gregory, L. A. Miller, J. R. Spence, J. F. Engelhardt, R. C. Boucher, J. R. Rock, S. H. Randell, P. R. Tata, Human distal lung maps and lineage hierarchies reveal a bipotent progenitor. *Nature* **604**, 111-119 (2022).
54. N. Frangogiannis, Transforming growth factor-β in tissue fibrosis. *J Exp Med* **217**, e20190103 (2020).
55. B. C. Willis, J. M. Liebler, K. Luby-Phelps, A. G. Nicholson, E. D. Crandall, R. M. du Bois, Z. Borok, Induction of epithelial-mesenchymal transition in alveolar epithelial cells by transforming growth factor-beta1: potential role in idiopathic pulmonary fibrosis. *Am J Pathol* **166**, 1321-1332 (2005).
56. M. Wijsenbeek, V. Cottin, Spectrum of Fibrotic Lung Diseases. *N Engl J Med* **383**, 958-968 (2020).
57. Y. M. Amrani, J. Gill, A. Matevossian, E. S. Alonzo, C. Yang, J. H. Shieh, M. A. Moore, C. Y. Park, D. B. Sant'Angelo, L. K. Denzin, The Paf oncogene is essential for hematopoietic stem cell function and development. *J Exp Med* **208**, 1757-1765 (2011).
58. F. J. Martinez, H. R. Collard, A. Pardo, G. Raghu, L. Richeldi, M. Selman, J. J. Swigris, H. Taniguchi, A. U. Wells, Idiopathic pulmonary fibrosis. *Nature Reviews Disease Primers* **3**, 17074 (2017).
59. A. Dobin, C. A. Davis, F. Schlesinger, J. Drenkow, C. Zaleski, S. Jha, P. Batut, M. Chaisson, T. R. Gingeras, STAR: ultrafast universal RNA-seq aligner. *Bioinformatics* **29**, 15-21 (2013).
60. G. La Manno, R. Soldatov, A. Zeisel, E. Braun, H. Hochgerner, V. Petukhov, K. Lidschreiber, M. E. Kastriti, P. Lönnerberg, A. Furlan, J. Fan, L. E. Borm, Z. Liu, D. van Bruggen, J. Guo, X. He, R. Barker, E. Sundström, G. Castelo-Branco, P. Cramer, I. Adameyko, S. Linnarsson, P. V. Kharchenko, RNA velocity of single cells. *Nature* **560**, 494-498 (2018).
61. V. Bergen, M. Lange, S. Peidli, F. A. Wolf, F. J. Theis, Generalizing RNA velocity to transient cell states through dynamical modeling. *Nat Biotechnol* **38**, 1408-1414 (2020).
62. G. S. Gulati, S. S. Sikandar, D. J. Wesche, A. Manjunath, A. Bharadwaj, M. J. Berger, F. Ilagan, A. H. Kuo, R. W. Hsieh, S. Cai, M. Zabala, F. A. Scheeren, N. A. Lobo, D. Qian, F. B. Yu, F. M. Dirbas, M. F. Clarke, A. M. Newman, Single-cell transcriptional diversity is a hallmark of developmental potential. *Science* **367**, 405-411 (2020).
63. B. Van de Sande, C. Flerin, K. Davie, M. De Waegeneer, G. Hulselmans, S. Aibar, R. Seurinck, W. Saelens, R. Cannoodt, Q. Rouchon, T. Verbeiren, D. De Maeyer, J. Reumers, Y. Saeys, S. Aerts, A scalable SCENIC workflow for single-cell gene regulatory network analysis. *Nat Protoc* **15**, 2247-2276 (2020).

## List of Supplementary Materials

**Fig. S1 to Fig. S14**

**Data file S1. Marker genes of each cell type in mouse lung scRNA-seq data.**
The list of marker genes for each cell type identity of mouse lung scRNA-seq data (GSE1412259), analyzed by the 'FindAllMarkers' function of Seurat.

**Data file S2. Marker genes of each cell type in human lung scRNA-seq.**
The list of marker genes for each cell type identity of human lung scRNA-seq data (GSE135893), analyzed by the 'FindAllMarkers' function of Seurat.

**Data file S3. Marker genes of each cell type in mouse lung scRNA-seq from *Pclaf* WT and *Pclaf* KO mice at 7 dpi of bleomycin.**
The list of marker genes for each cell type identity of *Pclaf* WT and KO mouse lung epithelial cells (collected from mice at 7 dpi of bleomycin instillation), analyzed by 'FindAllMarkers' function of Seurat.

**Data file S4. List of gene sets from of input into CLUE database.**
The list of gene sets of input into the CLUE database (*64*). Gene sets of the PPCs (*Pclaf* WT vs. *Pclaf* KO scRNA-seq shown in Figure 2). Gene sets of KP cells (*shPclaf* vs. *shControl [shCon]*) and H1792 cells (*shPCLAF* vs. *shControl [shCon]*) were identified from the bulk RNA-seq data (GSE136571 and GSE147305, respectively).

**Data file S5. List of drug candidates identified from the CLUE database.**
This spreadsheet has the output of the CLUE database with each gene sets. Each output was derived from the input gene sets listed in Supplementary Table 4; gene sets of PPCs (*Pclaf* WT vs. *Pclaf* KO), KP cells (*shPclaf* vs. *shControl [shCon]*) and H1792 cells (*shPCLAF* vs. *shControl [shCon]*). CLUE outputs (drug candidates) with scores higher than 1.5 were selected.

**Data file S6. Gene ontology of DREAM-target genes generated from the PANTHER database.**
The list of gene ontology (GO) (molecular function) of DREAM-target genes analyzed by the PANTHER db (*65*). The gene set of DREAM-target genes (968 genes; FISCHER_DREAM_TARGETS) was analyzed for the statistical overrepresentation test of GO molecular function complete.

**Data file S7. Antibody and primer information.**
This spreadsheet has all information related to antibodies (manufacturers, catalog numbers, dilution rates, and antigen retrieval methods) and primers (sequences for cloning and mRNA quantification).

## Supplementary References

64. A. Subramanian, R. Narayan, S. M. Corsello, D. D. Peck, T. E. Natoli, X. D. Lu, J. Gould, J. F. Davis, A. A. Tubelli, J. K. Asiedu, D. L. Lahr, J. E. Hirschman, Z. H. Liu, M. Donahue, B. Julian, M. Khan, D. Wadden, I. C. Smith, D. Lam, A. Liberzon, C. Toder, M. Bagul, M. Orzechowski, O. M. Enache, F. Piccioni, S. A. Johnson, N. J. Lyons, A. H. Berger, A. F. Shamji, A. N. Brooks, A. Vrcic, C. Flynn, J. Rosains, D. Y. Takeda, R. Hu, D. Davison, J. Lamb, K. Ardlie, L. Hogstrom, P. Greenside, N. S. Gray, P. A. Clemons, S. Silver, X. Y. Wu, W. N. Zhao, W. Read-Button, X. H. Wu, S. J. Haggarty, L. V. Ronco, J. S. Boehm, S. L. Schreiber, J. G. Doench, J. A. Bittker, D. E. Root, B. Wong, T. R. Golub, A Next Generation Connectivity Map: L1000 Platform and the First 1,000,000 Profiles. *Cell* **171**, 1437-+ (2017).

65. H. Mi, A. Muruganujan, X. Huang, D. Ebert, C. Mills, X. Guo, P. D. Thomas, Protocol Update for large-scale genome and gene function analysis with the PANTHER classification system (v.14.0). *Nat Protoc* **14**, 703-721 (2019).

# Fig. 1

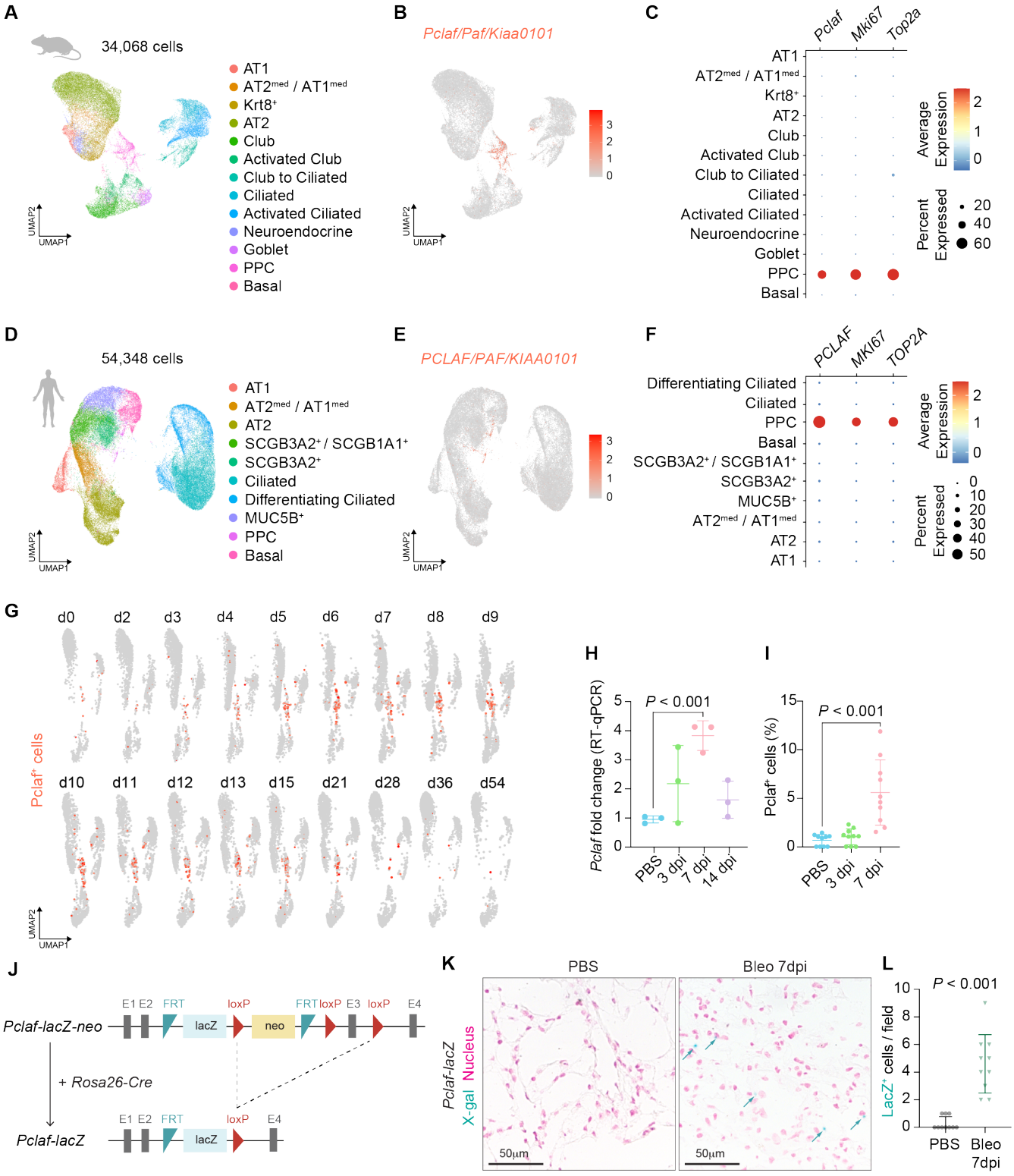


**Fig. 1. Pclaf$^{+}$ cells are elevated during lung regeneration.**

(**A** to **C**) A public scRNA-seq data set (GSE141259) was generated by subjecting sorted cells from the mouse lung epithelial compartment at 18 different time points after bleomycin instillation. (**A**) Uniform manifold approximation and projection (UMAP)-embedding displays cells colored by cell type identity. (**B**) Feature plot of *Pclaf* expression. (**C**) Dot plots showing *Pclaf*, *Mki67*, and *Top2a* gene expression in each cell type. (**D** to **F**) A public scRNA-seq data set (GSE135893) was generated from the human lung cells of 20 pulmonary fibrotic diseases and 10 control lungs. (**D**) UMAP embedding displays cells colored by cell type identity. (**E**) Feature plot

of expression of *PCLAF*. (**F**) Dot plots for *PCLAF*, *MKI67*, and *TOP2A* gene expression in each cell type. (**G**) Feature plots of *Pclaf* expression in mouse lung at the indicated time points using data shown in Fig 1A. (**H** and **I**) Mouse lungs ($n$ = 3) were collected after bleomycin (1.4 U/kg) had been added to the trachea at the indicated time points. (**H**) RT-qPCR analysis of the *Pclaf* mRNA level. Hprt was used as an internal control. (**I**) Quantification of $Pclaf^{+}$ cells by immunostaining. (**J**) Scheme of establishing *Pclaf-lacZ* knock-in mice. The neo cassette was deleted by breeding *Pclaf-lacZ-neo* with Rosa26-Cre driver. (**K**) Representative images of X-gal staining. *Pclaf-lacZ* mice were instilled with bleomycin (1.4 U/kg) or PBS (0 dpi). After 7 dpi, lungs were collected and stained for X-gal (5-bromo-4-chloro-3-indolyl-β-D-galactopyranoside; blue) and nuclear fast red (pink). (**L**) Quantification of $lacZ^{+}$ cells. Two-tailed Student's *t*-test; error bars: standard deviation (SD). The represented data are shown (n>=3).

# Fig. 2

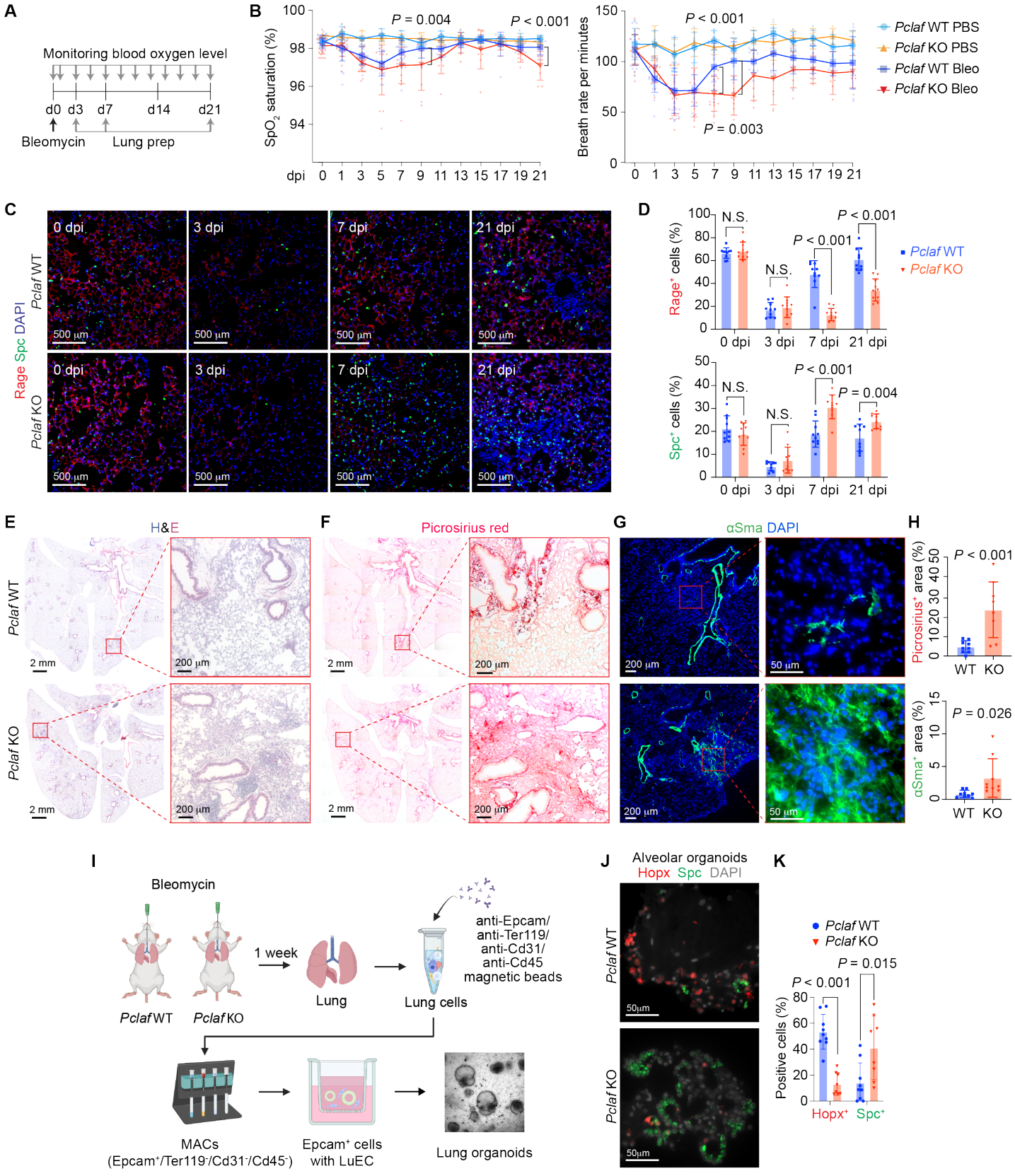


**Fig. 2. *Pclaf* KO impairs lung regeneration.**

(**A**) Experimental scheme for the bleomycin-induced lung injury model. *Pclaf* WT and KO mice were treated with phosphate-buffered saline (PBS) (n = 5 for *Pclaf* WT, n = 5 for *Pclaf* KO) or bleomycin (1.4 U/kg; n = 25

for *Pclaf* WT, n = 24 for *Pclaf* KO) by intratracheal instillation. The blood oxygen level ($SpO_2$) and breath rate were measured by pulse-oximetry at the indicated time points. At 3 days after injury (dpi, n = 7 for each group with bleomycin), 7 dpi (n = 8 for each group with bleomycin), and 21 dpi (n = 10 for *Pclaf* WT, n = 8 for *Pclaf* KO with bleomycin, n = 5 for each group with PBS (0 dpi)), the lungs were collected for further analysis. (**B**) The dynamics of $SpO_2$ levels (*left* panel) and breath rate per minute (*right* panel) were measured at the indicated time points. (**C** and **D**) Representative images (**C**) and quantification graph (**D**) of immunostaining for Rage (red; AT1) and Spc (green; AT2) at the indicated time points. (**E**) Representative images of hematoxylin and eosin (H&E) staining at 21 dpi. (**F**) Representative images of picrosirius staining (collagen fiber) at 21 dpi. (**G**) Representative images of immune-staining for alpha-smooth muscle actin (αSMA/Acta2; smooth muscle cell) at 21 dpi. (**H**) Quantification graphs of the picrosirius$^+$ area (*upper* panel) and αSMA$^+$ area (*bottom* panel). (**I** to **K**) The lung epithelial cells were isolated from bleomycin-treated lungs of *Pclaf* WT or *Pclaf* KO mice at 7 dpi by magnetic-activated cell sorting (MACS). The lung epithelial cells (Ter119$^-$/Cd31$^-$/Cd45$^-$/Epcam$^+$) were cultured with lung endothelial cells (Cd31$^+$) at a liquid-air interface to generate LOs. (**I**) Scheme of LO culture. (**J**) Images of alveolar type organoids fluorescently immunostained for Hopx (red; AT1) and Spc (green; AT2). (**K**) Quantification graph of Hopx$^+$ and Spc$^+$ cells. Two-tailed Student's *t*-test; error bars: SD. The represented images are shown (n>=3).

## Fig. 3

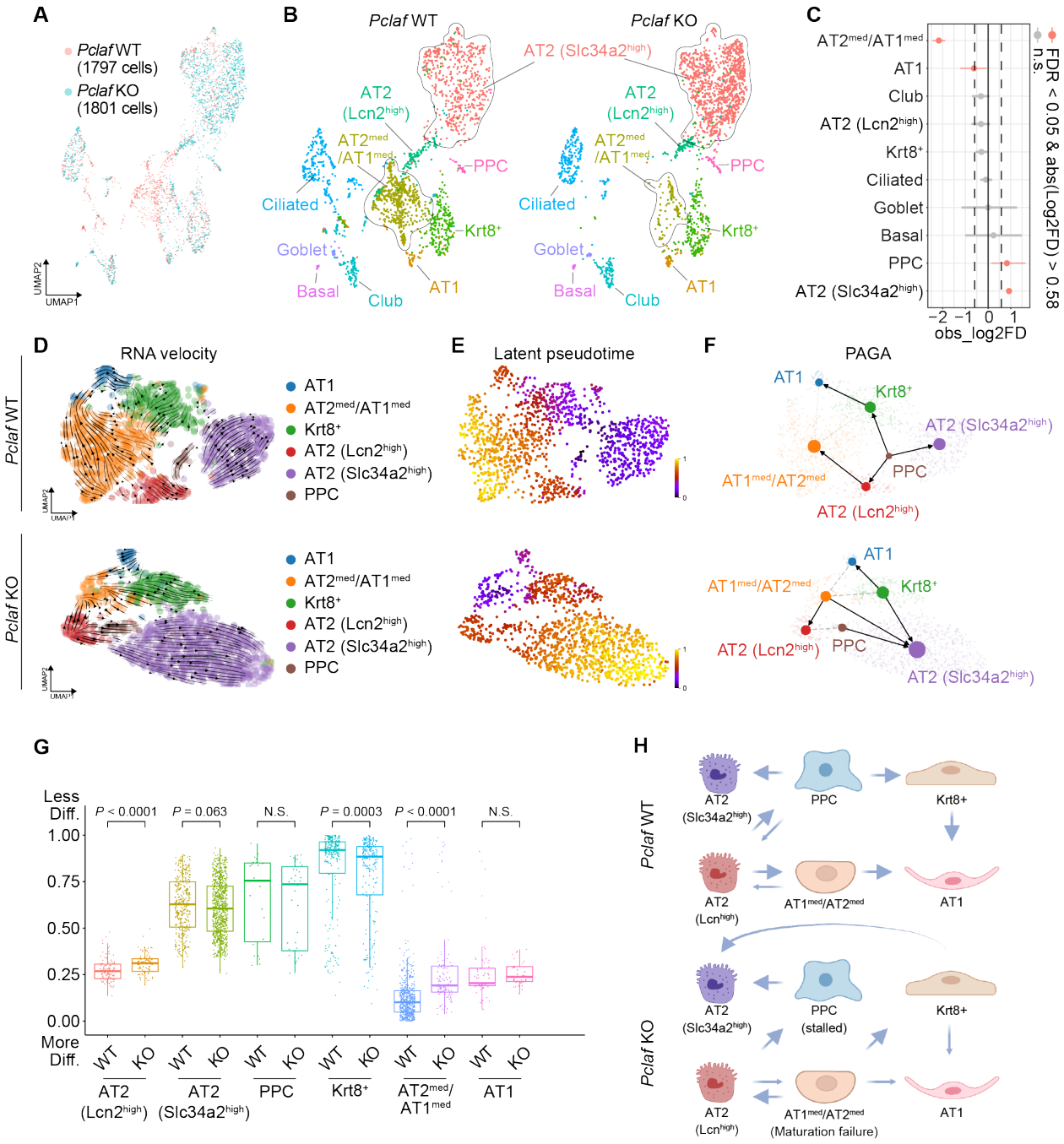


**Fig. 3. *Pclaf* KO suppresses AT2 cell lineage plasticity.**
(**A**) Integrated UMAP displaying each cell cluster of pulmonary epithelial cells isolated from *Pclaf* WT and KO mice. (**B**) UMAPs (split by *Pclaf* WT and KO) displaying each cell cluster, colored by cell types. (**C**) Cell proportion analysis of *Pclaf* WT vs. KO by cell type. (**D** to **F**) RNA velocity analyses (**D**), latent pseudotime analysis (**E**), and PAGA analysis (**F**) of *Pclaf* WT (*upper* panels) or KO (*bottom* panels) based on scRNA-seq are depicted. (**G**) Boxplots of predicted cluster-differentiation based on the CytoTRACE analysis. (**H**) Illustration of cellular trajectories in *Pclaf* WT (*upper* panel) or KO (*bottom* panel) cells during lung regeneration.

# Fig. 4

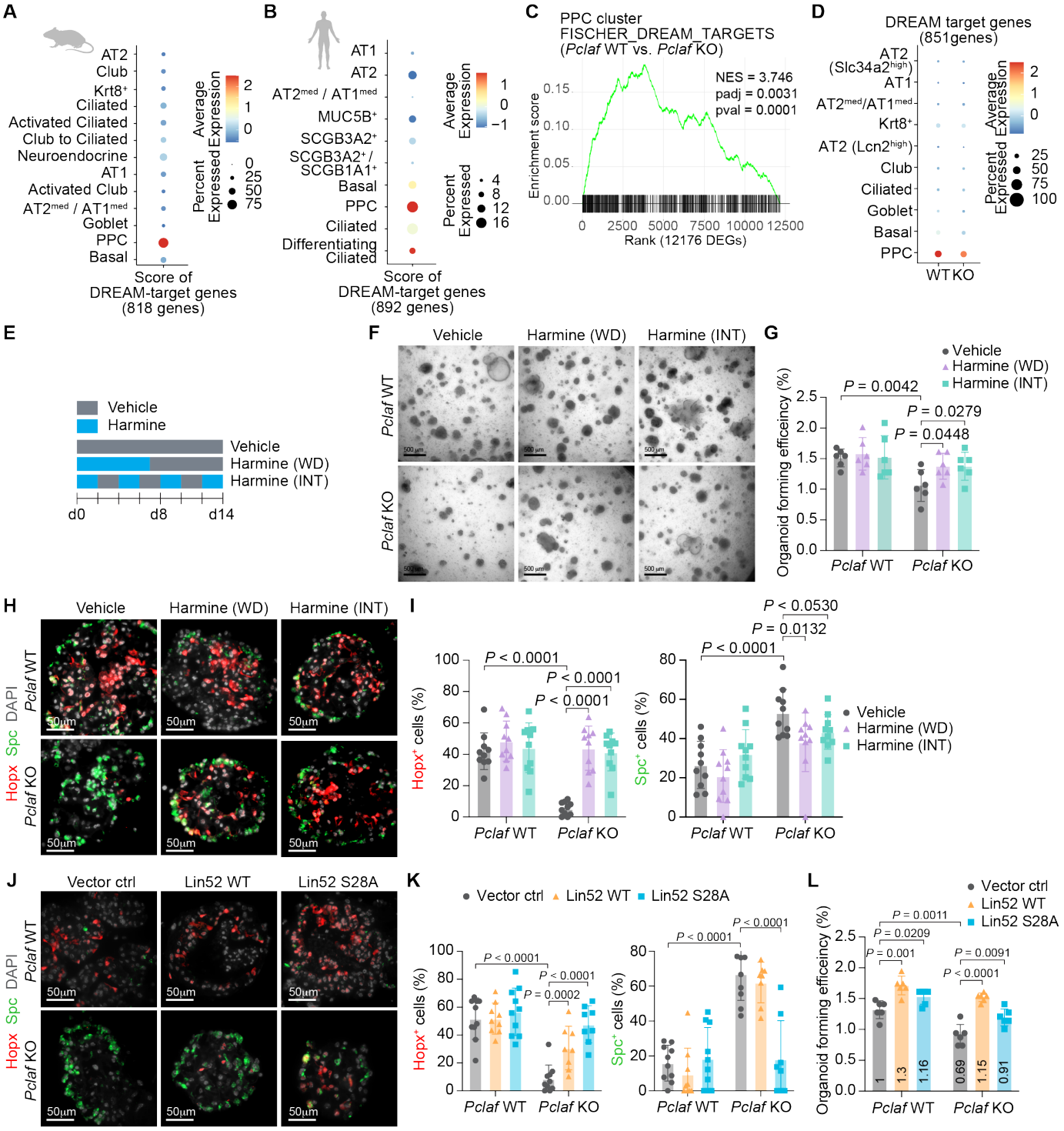


**Fig. 4. PCLAF-DREAM axis mediates AT2 cell lineage plasticity for lung regeneration.**
(**A**) Dot plots depicting transcriptional module scores of the gene sets of DREAM-target genes with the mouse scRNA-seq dataset shown in Fig. 1A. (**B**) Dot plots depicting transcriptional module scores of the gene sets of DREAM-target genes with the human scRNA-seq data set shown in Fig. 1D. (**C**) Gene set enrichment analysis (GSEA) of *Pclaf* WT vs. *Pclaf* KO in the PPC cluster using the data set shown in Fig. 3. The enrichment plot presents the gene sets of DREAM-target genes. (**D**) Dot plots depicting transcriptional module scores of the DREAM-target gene set using the data set shown in Figure 2. (**E**) Experimental scheme for LO culture under

stimuli of harmine (200 nM). Harmine was used to treat LOs for the first 7 days and withdrawn (WD). Alternatively, LOs were cultured with harmine intermittently (INT) at the indicated time points. (**F**) The representative bright-field z-stack images of LOs on day 12. (**G**) Quantification graph of lung OFE. (**H**) Representative images of IF staining for Hopx (AT1; red) and Spc (AT2; green) on day 14. (**I**) Quantification graph of $Hopx^+$ and $Spc^+$ cells. (**J** to **L**) Isolated lung epithelial cells were transduced with RFP, Lin52 WT, or Lin52 S28A by lentivirus and then cultured with LO. (**J**) Representative images of IF staining for Hopx (AT1; red) and Spc (AT2; green) on day 14. (**K**) Quantification graph of $Hopx^+$ and $Spc^+$ cells. (**L**) Quantification graph of lung OFE. Two-tailed Student's *t*-test; error bars: SD. The represented images and data are shown (n>=3).

# Fig. 5

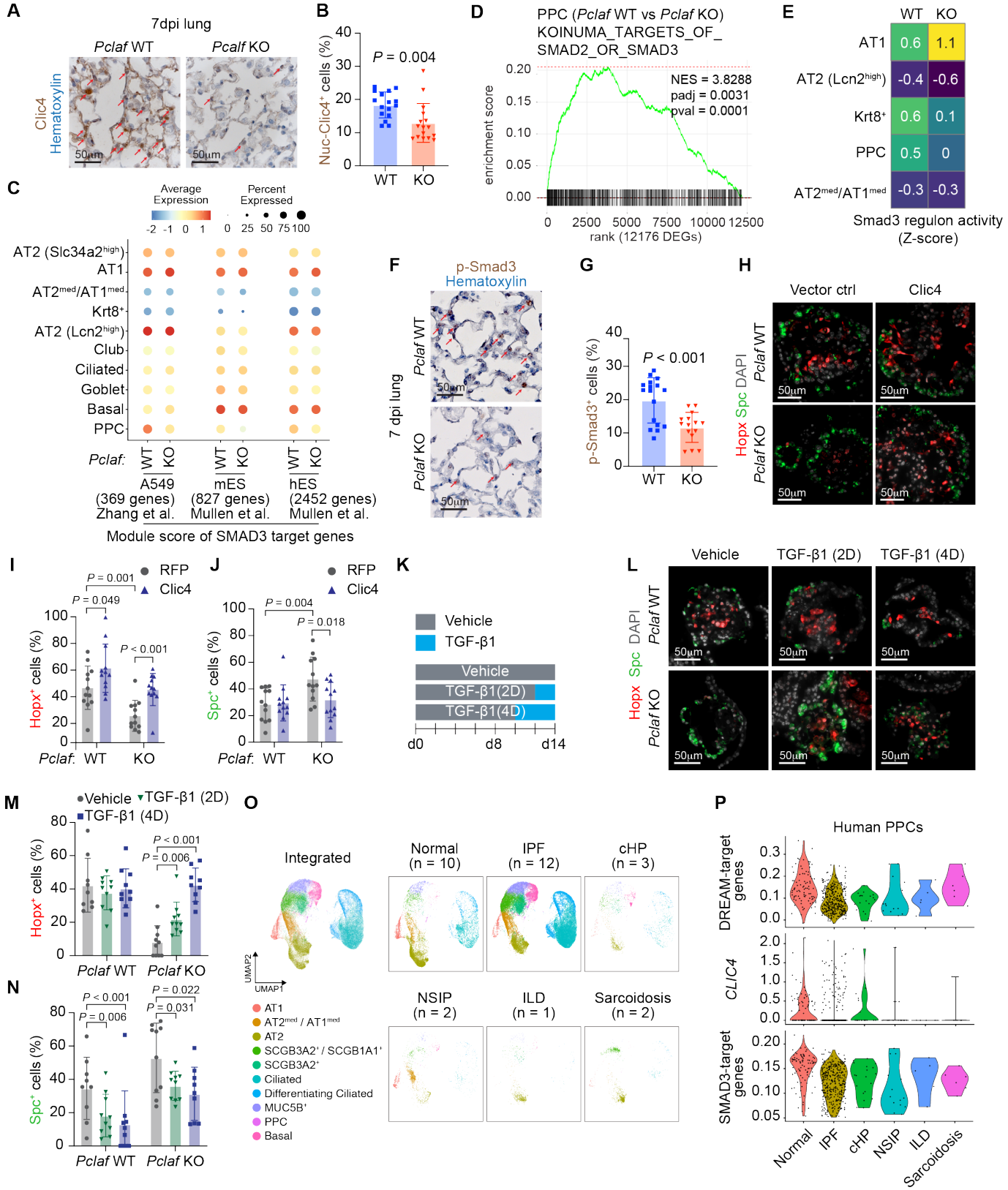


**Fig. 5. PCLAF-DREAM-mediated CLIC4-TGF-β signaling axis is required for AT1 cell differentiation.** (**A**) Representative images of *Pclaf* WT and *Pclaf* KO lung at 7 dpi, chemically immunostained for Clic4. (**B**) Quantification graph of nucleus Clic4$^+$ cells. (**C**) Dot plots depicting transcriptional module scores of SMAD3 gene sets from A549, mouse embryonic stem cells (mES), and human embryonic stem cells (hES) using the

scRNA-seq dataset shown in Fig. 3. (**D**) GSEA of *Pclaf* WT vs. *Pclaf* KO in the PPC cluster using the data set shown in Fig. 3. The enrichment plot presents the gene sets of SMAD2 or SMAD3 target genes. (**E**) Z-score of Smad3 regulon activity by cell type and genome, analyzed by pySCENIC using the data set shown in Fig. 3. (**F**) Representative images of *Pclaf* WT and *Pclaf* KO lung at 7 dpi, chemically immunostained for p-Smad3. (**G**) Quantification graph of p-Smad3$^{+}$ cells. (**H** to **J**) Isolated lung epithelial cells were transduced with RFP- or CLIC4-expressing lentiviruses and cultured with LO. (**H**) Representative images of IF staining for Hopx (AT1; red) and Spc (AT2; green) on day 14. (**I** and **J**) Quantification of Hopx$^{+}$ (**I**) and Spc$^{+}$ cells (**J**). (**K** to **N**) *Pclaf* WT, or KO lung epithelial cells-derived LOs were cultured with TGF-β1 (2 ng/ml) for 2 days (TGFβ1 [2D]) or 4 days (TGFβ1 [4D]). (**K**) Experimental scheme for TGF-β1 treatment. **l**, Representative images of IF staining for Hopx (AT1; red) and Spc (AT2; green) on day 14. (**M** to **N**) Quantification of Hopx$^{+}$ (**M**) and Spc$^{+}$ cells (**N**). (**O**) UMAP plots displaying each cell cluster from the scRNA-seq datasets of normal human lung and fibrotic diseases shown in Fig. 1D. (IPF; idiopathic pulmonary fibrosis, cHP; chronic hypersensitivity pneumonitis, NSIP; nonspecific interstitial pneumonia, ILD; interstitial lung disease). (**P**) Violin plots showing the expression of module scores of DREAM-target genes, *CLIC4* expression, and hES-SMAD3-target genes in the PPC clusters from the human scRNA-seq data set. Two-tailed Student's *t*-test; error bars: SD. The represented images are shown (n>=3).

## Fig. 6

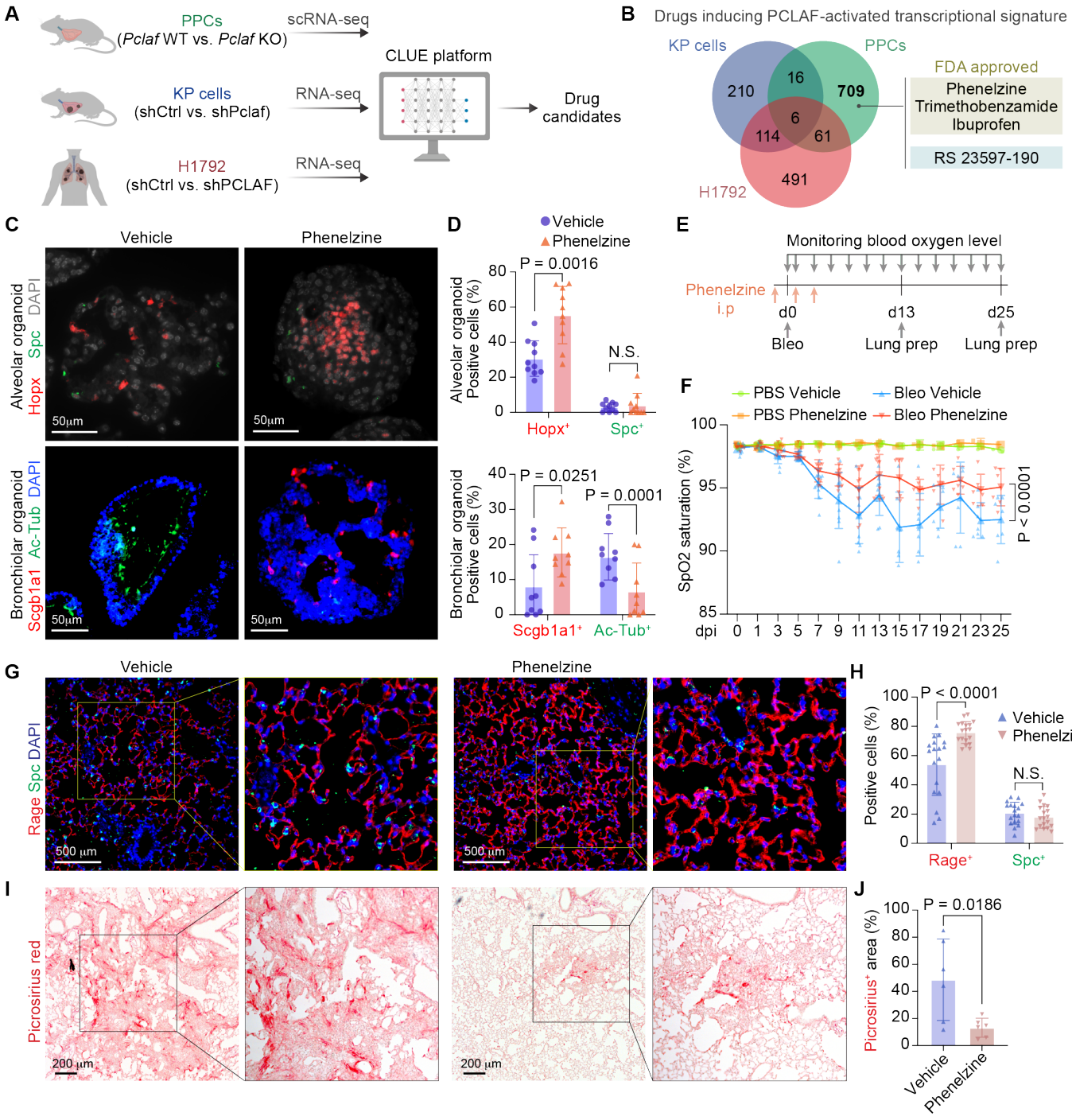


**Fig. 6. Pharmacological mimicking of PCLAF-DREAM-activated transcriptional signature restores lung regeneration.**

(**A**) Experimental scheme to identify drug candidates by the CLUE platform. (**B**) Venn diagram of Connectivity Map results, identifying drug candidates specific to normal lung PPCs. (**C**) Representative images of LOs with phenelzine (10 μM) that fluorescently immunostained for Hopx (AT1; red; *upper* panels), Spc (AT2; green; *upper* panels), Scgb1a1 (Club; red; *bottom* panels), and Ac-Tub (Ciliated; green; *bottom* panels). (**D**) Quantification graph of Hopx$^+$ (*upper* panel), Spc$^+$ (*upper* panel), Scgb1a1$^+$ (*bottom* panel), and Ac-Tub$^+$ (*bottom* panel) cells. (**E**) Experimental scheme for bleomycin-induced lung regeneration by phenelzine. Mice were treated with bleomycin (2.8 U/kg) by intratracheal instillation. The vehicle control (DMSO, n = 10) or phenelzine (n = 10; 750 μg/head) were administered by intraperitoneal injection at -1, 1, and 3 dpi. The blood oxygen level ($SpO_2$)

and breath rate were measured by pulse oximetry every other day. At 13 dpi (n = 4 for each group) and 25 dpi (n = 6 for each group), lungs were collected for further analysis. (**F**) The dynamics of $spO_2$ levels were measured at the indicated time points. Two-way ANOVA with post-hoc Tukey test. (**G**) Representative images of the lungs at 13 dpi, fluorescently immunostained for Rage (AT1; red) and Spc (AT2; green). (**H**) Quantification graph of $Rage^+$ or $Spc^+$ cells. (**I**) Representative images of picrosirius staining at 25 dpi. (**J**) Quantification graphs of the $picrosirius^+$ area. Two-tailed Student's *t*-test except for Figure 5f; error bars: SD. The representative images are shown (n>=3).

# Fig. S1

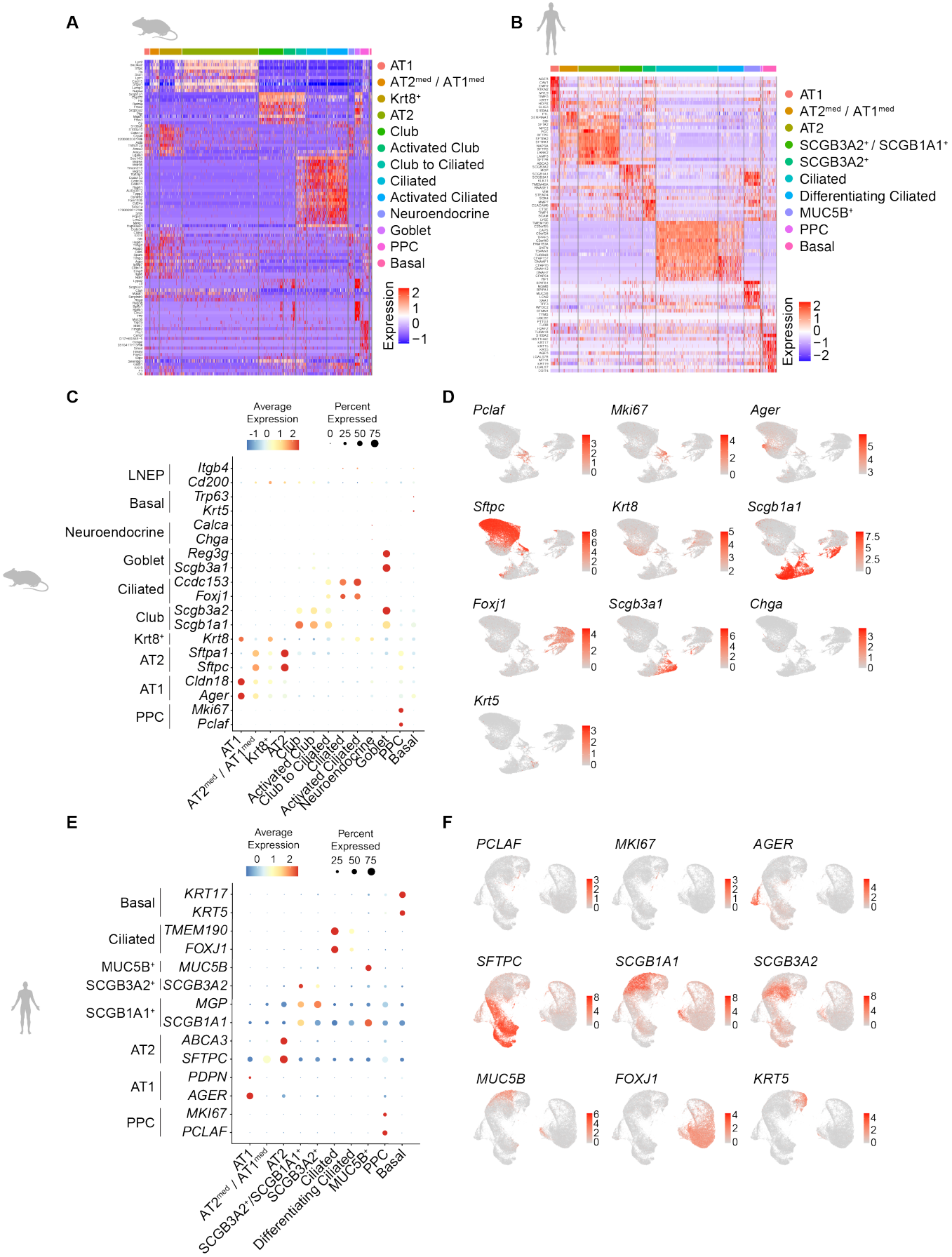


**Fig. S1. The cell type annotation of human and mouse lung single-cell transcriptomics.**

(**A**) Heatmap of gene expression of the top 10 genes in each cell type of mouse lung using data shown in Fig. 1A. (**B**) Heatmap of gene expression of the top 10 genes in each cell type of human lung using data shown in Fig. 1D. (**C**) Dot plots for mouse lung epithelial marker gene expression in each cell type. (**D**) Feature plots of mouse lung epithelial marker gene expression. (**E**) Dot plots for human lung epithelial marker gene expression in each cell type. (**F**) Feature plots of human lung epithelial marker gene expression.

## Fig. S2

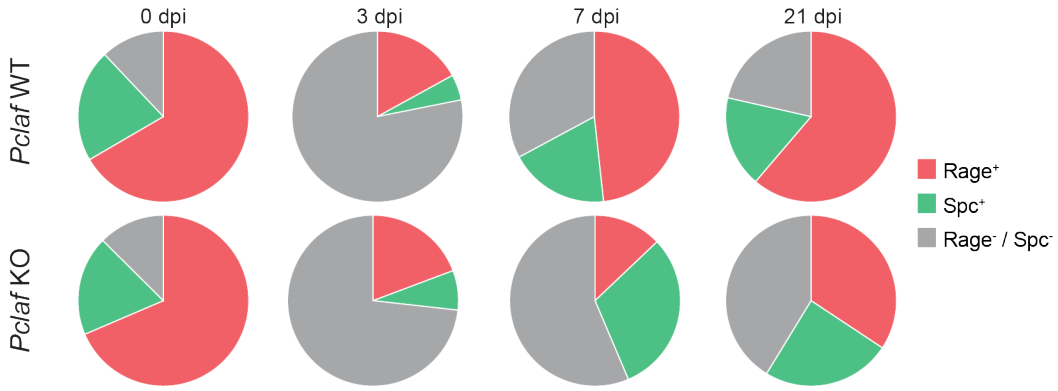


**Fig. S2. *Pclaf* KO inhibits AT1 regeneration and promotes AT2 repopulation.**
Pie plots of Rage$^+$ (AT1) and Spc$^+$ (AT2) cells using data shown in Fig. 1C.

# Fig. S3

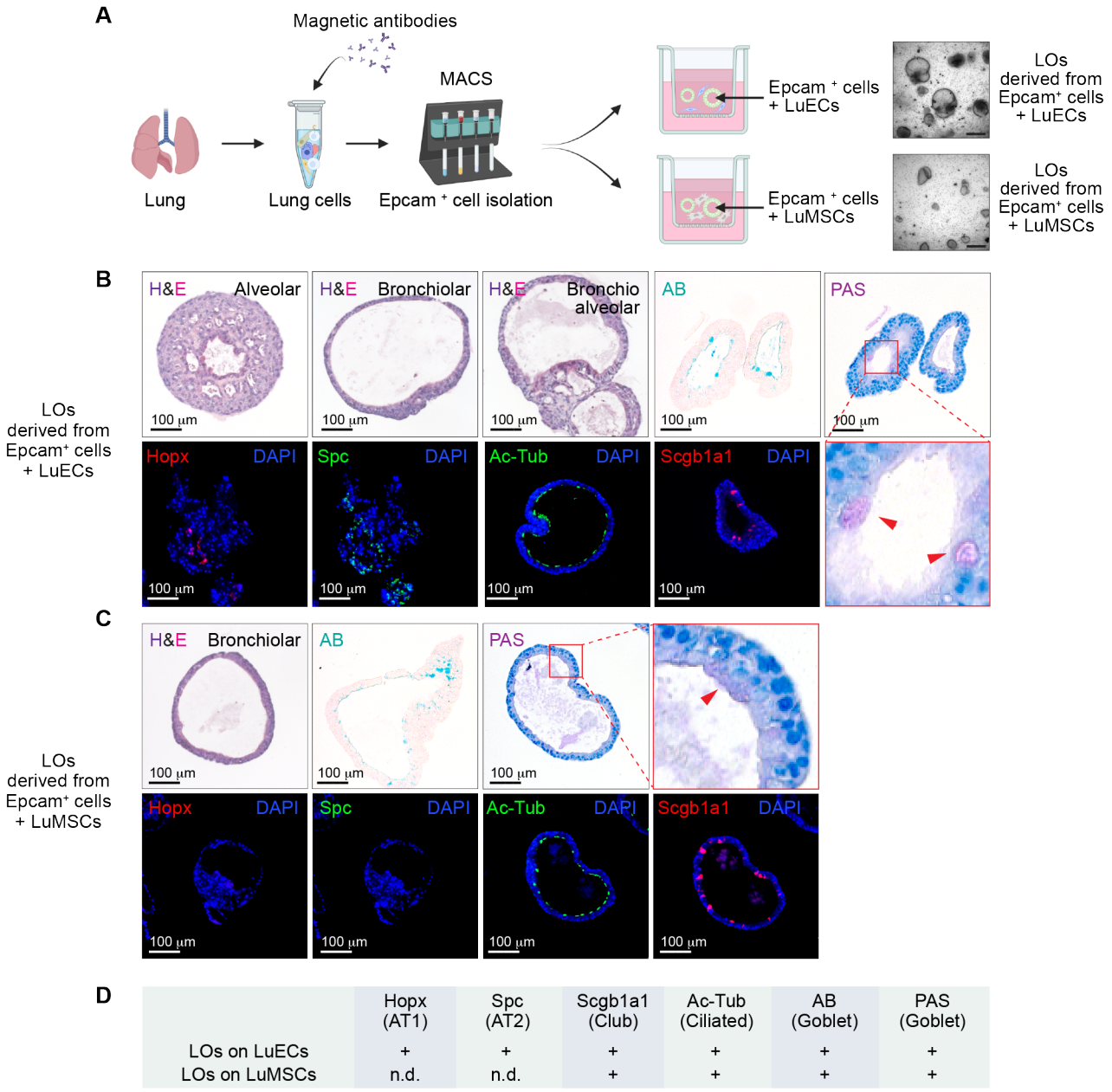


D

| | Hopx (AT1) | Spc (AT2) | Scgb1a1 (Club) | Ac-Tub (Ciliated) | AB (Goblet) | PAS (Goblet) |
|---|---|---|---|---|---|---|
| LOs on LuECs | + | + | + | + | + | + |
| LOs on LuMSCs | n.d. | n.d. | + | + | + | + |

**Fig. S3. Comparison of LO culture systems.**
(**A**) Scheme of LO culture. The lung epithelial cells were isolated from WT mice by MACS and cultured with LuECs or LuMSCs at a liquid-air interface to grow LOs. (**B** and **C**) Representative images of organoids for hematoxylin and eosin (H&E), alcian blue (AB), and periodic acid-Schiff (PAS) staining (*upper* panels), and immunostained for Hopx (AT1), Spc (AT2), Ac-Tub (Ciliated), and Scgb1a1 (Club; *bottom* panels) of organoids with LuECs (**B**) and with LuMSCs (**C**). (**D**) Table of positive cells using data shown in Fig S3B and C. The represented images are shown (n>=3).

# Fig. S4

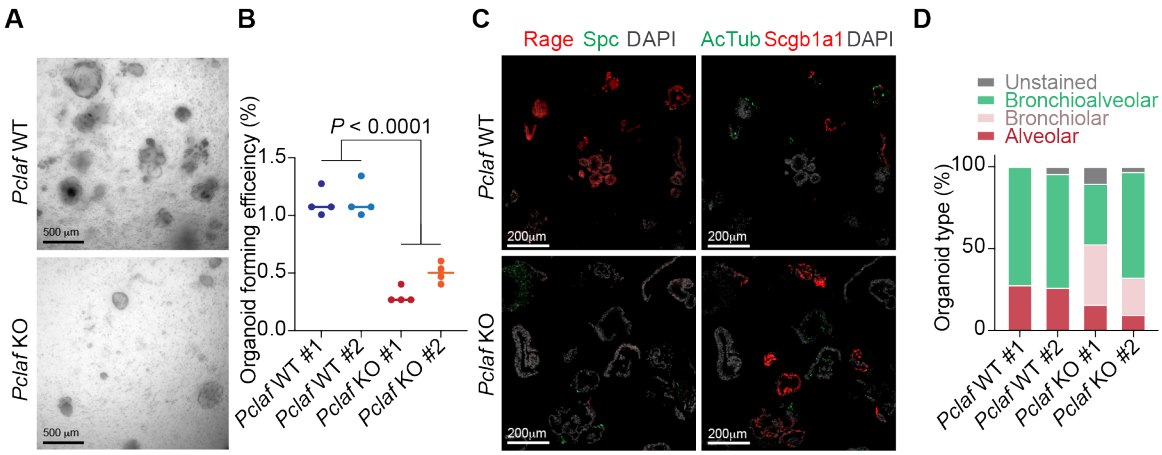


**Fig. S4. *Pclaf* KO inhibits alveolar-type lung organoid formation.**
(**A** to **D**), The lung epithelial cells were isolated from bleomycin-treated lungs of *Pclaf* WT or *Pclaf* KO mice at 7 dpi (bleomycin administration) by magnetic-activated cell sorting (MACS). The lung epithelial cells ($Ter119^-$/$Cd31^-$/$Cd45^-$/$Epcam^+$) were cultured with lung endothelial cells ($Cd31^+$) at a liquid-air interface to generate LOs. (**A**) Bright-field z-stack images of LOs at day 12. (**B**) Quantification graph of lung OFE. (**C**) Representative images of LOs that were fluorescently immunostained for Rage (AT1; red; *left* panels), Spc (AT2; green; *left* panels), acetyl-Tubulin (Ciliated; AcTub; green; *right* panels), and Scgb1a1 (Club; red; *right* panels). (**D**) Quantification graph of organoid type. Two-tailed Student's *t*-test; error bars: SD. The represented images and data are shown (n>=3).

# Fig. S5

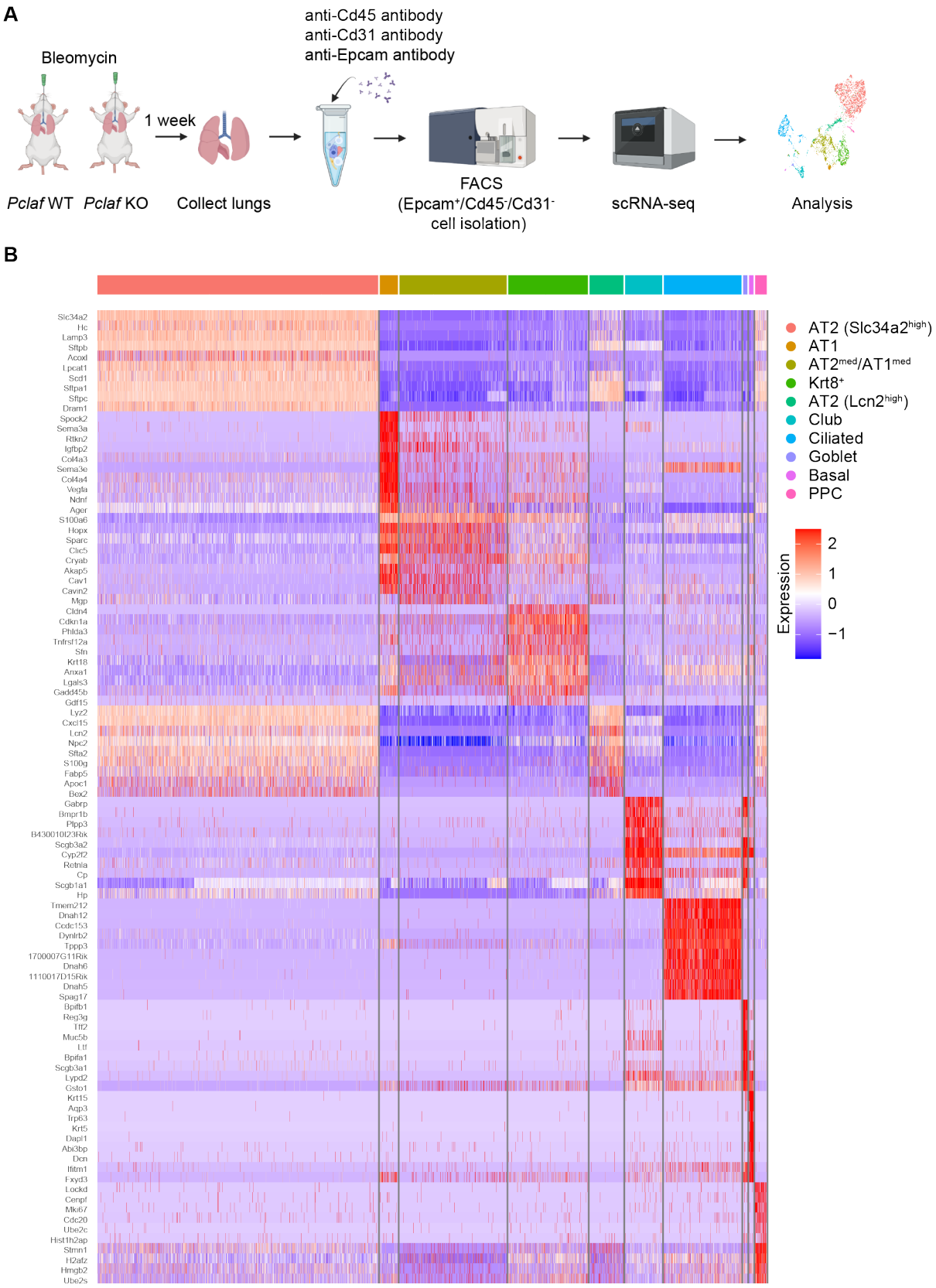


**Fig. S5. Scheme of single-cell transcriptomics of *Pclaf* WT and KO mouse lung tissues.**

(**A**) Scheme of scRNA-seq. Lung epithelial cells were isolated from *Pclaf* WT and KO mice (treated with bleomycin) by fluorescence-activated cell sorting (FACS). $CD31^{-}/CD45^{-}/Epcam^{+}$ cells were used to generate sequencing data using the 10X genomics single-cell sequencing service. (**B**) Heatmap of gene expression-based cell clusters of the top 10 genes in each cell type of mouse lung using data shown in Fig. 3B.

# Fig. S6

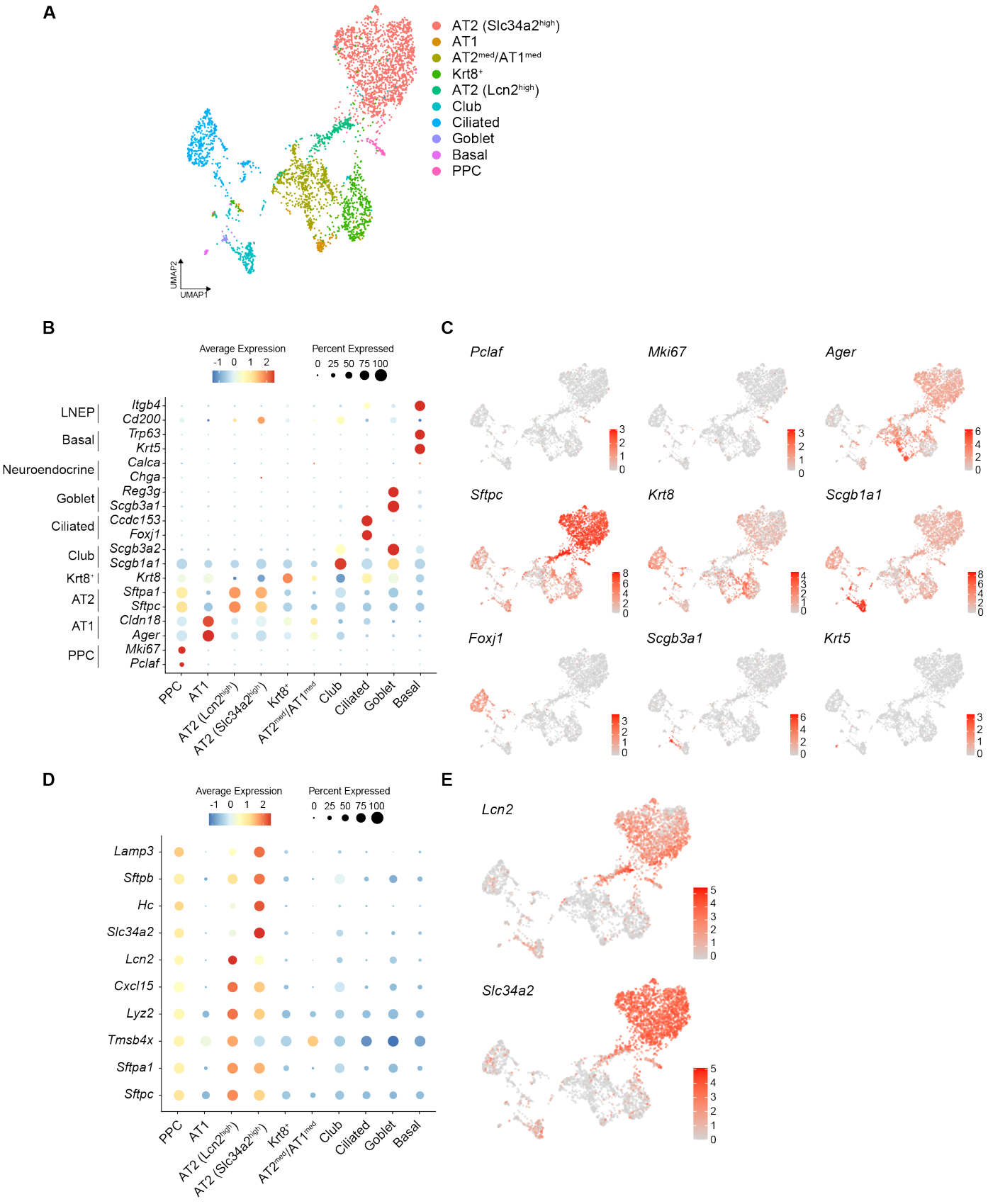


**Fig. S6. Cell type annotation of mouse lung single-cell transcriptomics.**
Analysis of the scRNA-seq dataset is shown in Fig. 3B. (**A**) UMAP displays each cell cluster, colored by cell type. (**B**) Dot plots for mouse lung epithelial marker gene expression quantification of each cell type. (**C**) Feature

plots of mouse lung epithelial marker gene expression. (**D**) Dot plots for genes specifically expressed in AT2(Lcn$^{high}$) and AT2(Slc34a$^{high}$). (**E**) Feature plots displaying the expression of *Lcn2* and *Slc34a2*.

# Fig. S7


**Fig. S7. *Pclaf* KO downregulates DREAM-target gene expression in PPC.**
(**A**) Venn diagram analysis of DREAM target genes vs. genes specifically expressed in the PPC clusters (mouse scRNA-seq dataset shown in Fig. 1A or the human scRNA-seq dataset shown in Fig. 1D). (**B**) Top 20 gene sets (*upper* panel) and bottom 20 gene sets (*bottom* panel) of GSEA with 12,176 DEGs between *Pclaf* WT PPCs and *Pclaf* KO PPCs.

# Fig. S8

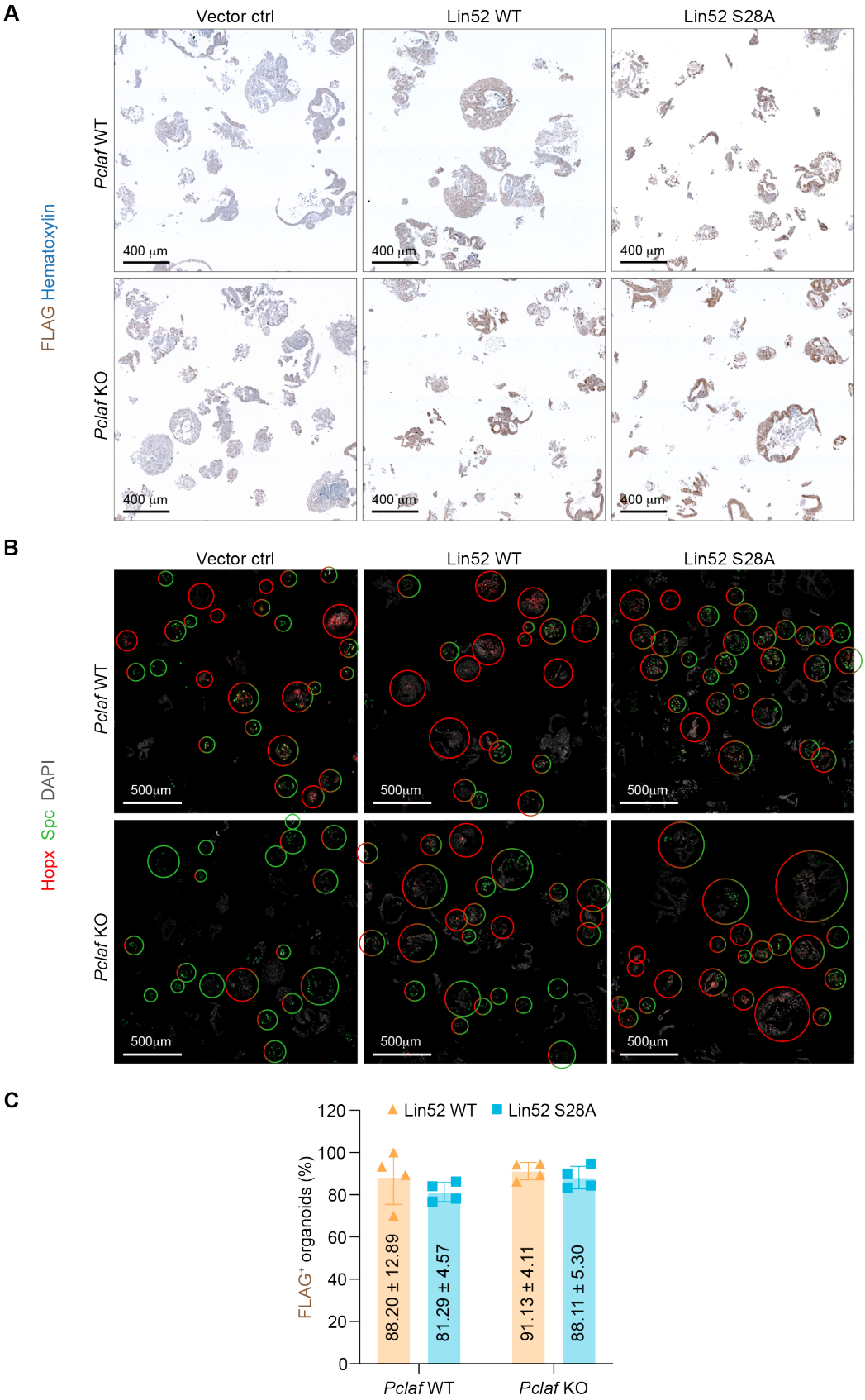


**Fig. S8. Transduction efficiency of lentiviruses encoding Lin52-WT or Lin52 S28A in LOs.**

Isolated lung epithelial cells were transduced with RFP, Lin52 WT, or Lin52 S28A by lentivirus and then cultured with LO. (**A**) Representative images chemically immunostained for FLAG. (**B**) Representative images of IF staining for Hopx (AT1; red) and Spc (AT2; green) on day 14. The circles (in red-green mixed) indicate the relative ratio of $Hopx^+$ to $Spc^+$ cells in LOs. (**C**) Quantification of $FLAG^+$ LOs. The represented images and data are shown (n>=3); error bars: SD.

# Fig. S9

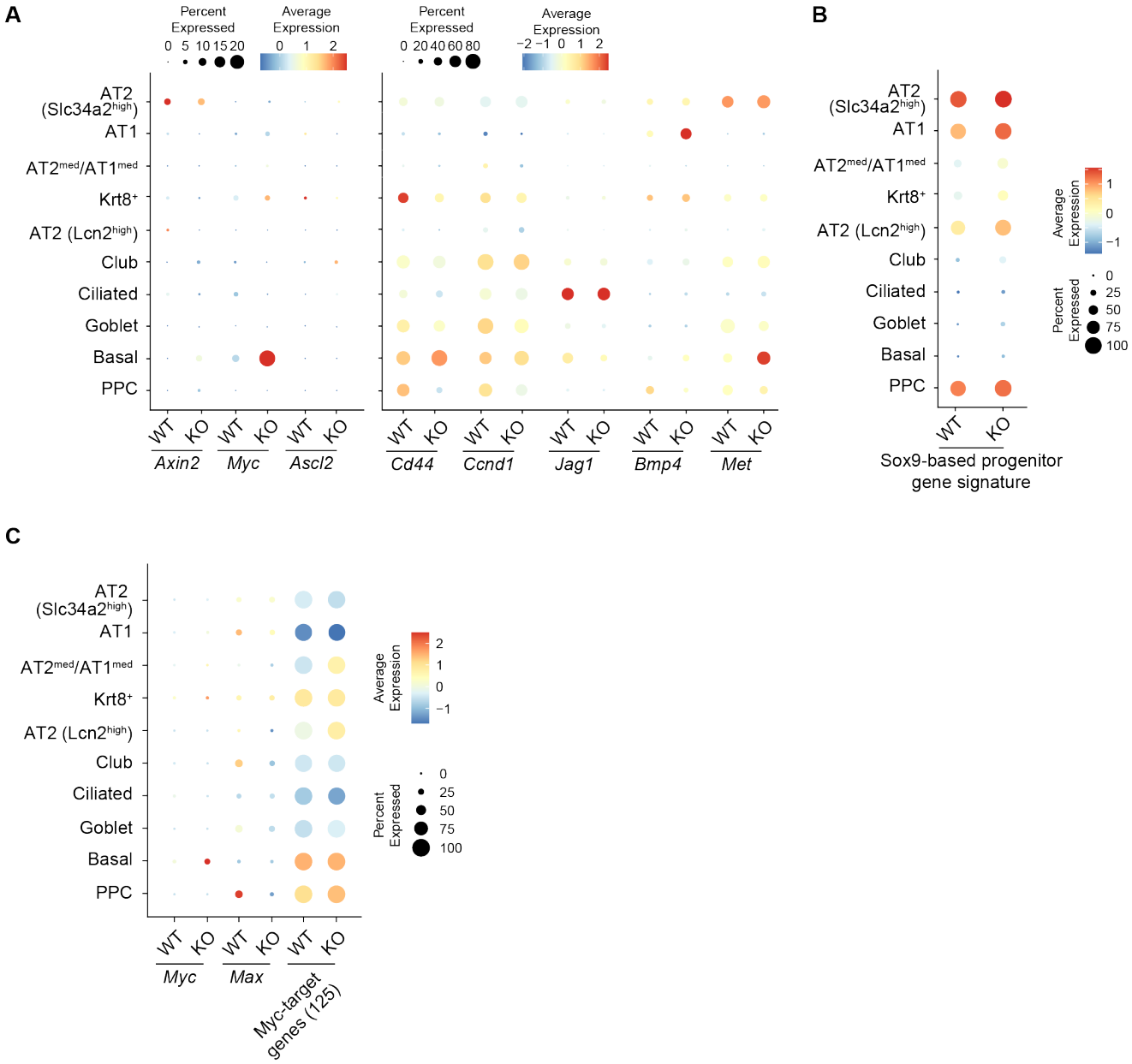


**Fig. S9. Impact of *Pclaf* KO on Wnt signaling, Sox9, and Myc transcriptional signatures.**
(**A** to **C**) Dot plots displaying each gene expression from the scRNA-seq dataset shown in Fig. 3. (**A**) Dot plots showing the expression of Wnt signaling target genes in each cell type. (**B**) Dot plots depicting transcriptional module scores of the Sox9-based progenitor cell signature gene set. (**C**) Dot plots showing the expression of *Myc* and *Max* and transcriptional module scores of the Myc-target gene set. Of note, *Pclaf* KO barely alters Wnt signaling and Sox9-based progenitor transcriptional signature.

# Fig. S10

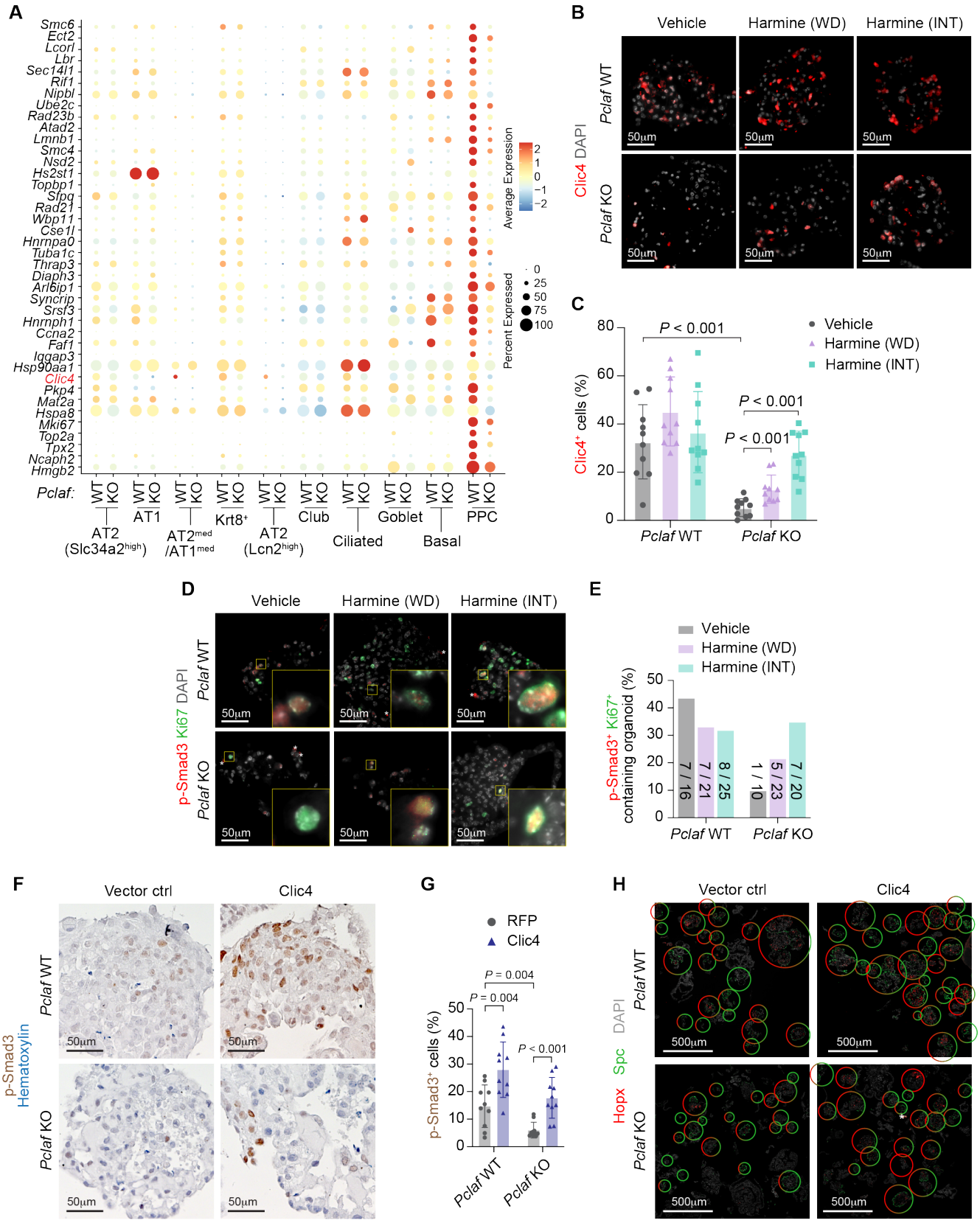


**Fig. S10. Pharmacological or genetic activation of the DREAM axis rescues *Pclaf* KO-inhibited TGF-β signaling.**

(**A**) Dot plots displaying the top 40 differently expressed DREAM target genes in each cell type. (**B** to **E**) LOs treated with harmine (shown in Fig. 3E) were immunostained with indicated antibodies. (**B**) Representative

images of IF staining for Clic4 (red). (**C**) Quantification of the Clic4$^+$ cells. (**D**) Representative images of IF staining for p-Smad3 (red) and Mki67 (green) on day 14. (**E**) Quantification of LOs containing p-Smad3 and Mki67 double-positive cells. (**F** to **J**) Isolated lung epithelial cells were transduced with RFP- or CLIC4-expressing lentiviruses and cultured with LO. (**F**) Representative images of *Pclaf* WT and *Pclaf* KO LOs at day 14, chemically immunostained for p-Smad3. (**G**) Quantification graph of p-Smad3$^+$ cells. (**H**) Images of IF staining for Hopx (AT1; red) and Spc (AT2; green) on day 14. The circle color indicates the relative ratio of Hopx$^+$ to Spc$^+$ cells. Two-tailed Student's *t*-test; error bars: SD. The representative images are shown (n>=3).

## Fig. S11

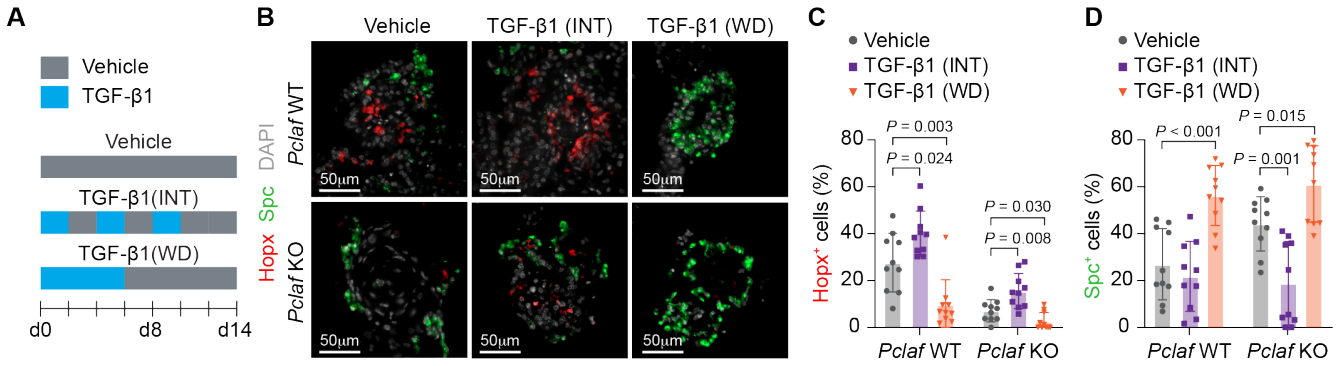


**Fig. S11. TGF-β rescues *Pclaf* KO-impaired cell plasticity.**

(**A** to **D**) Murine lung epithelial cells were cultured for LOs under stimuli of TGF-β1 (2 ng/ml). TGF-β1 was used to treat LOs for the first 6 days and withdrawn (WD). Alternatively, LOs were cultured with TGF-β1 intermittently (INT) at the indicated time points. (**A**) Experimental scheme for LO culture. (**B**) Representative images of IF staining for Hopx (AT1; red) and Spc (AT2; green) on day 14. (**C** and **D**) Quantification of $Hopx^+$ (**C**) and $Spc^+$ cells (**D**). Two-tailed Student's *t*-test; error bars: SD. The representative images are shown (n>=3). TGF-β1 (INT) rescued *Pclaf* KO-impaired alveolar cell plasticity (AT1 cell generation from AT2 cells). In contrast, TGF-β1 (WD) inhibited AT1 cell generation regardless of *Pclaf* WT and *Pclaf* KO. These data suggest that the temporal activity of TGF-β signaling is pivotal for AT2-to-AT1 cell transition.

## Fig. S12

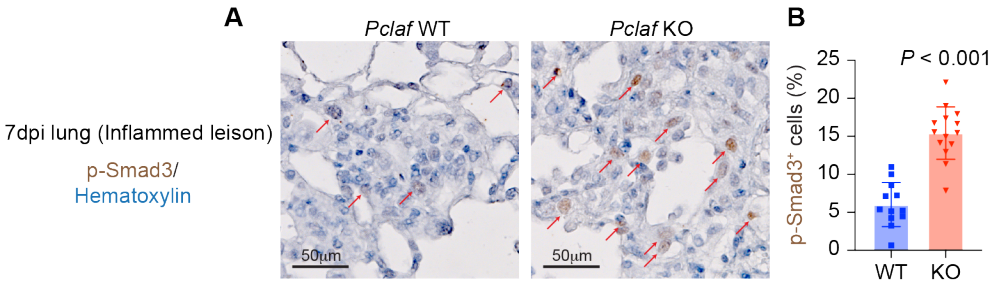


**Fig. S12. Elevated TGF-β signaling in inflamed lesions by *Pclaf* KO.**
(**A**) Images of immunostaining for p-Smad3 of the inflamed lesion from *Pclaf* WT and *Pclaf* KO lung tissues at 7 dpi. (**B**) Quantification graph of p-Smad3$^{+}$ cells. Two-tailed Student's *t*-test; error bars: SD. The representative images are shown (n>=3).

## Fig. S13

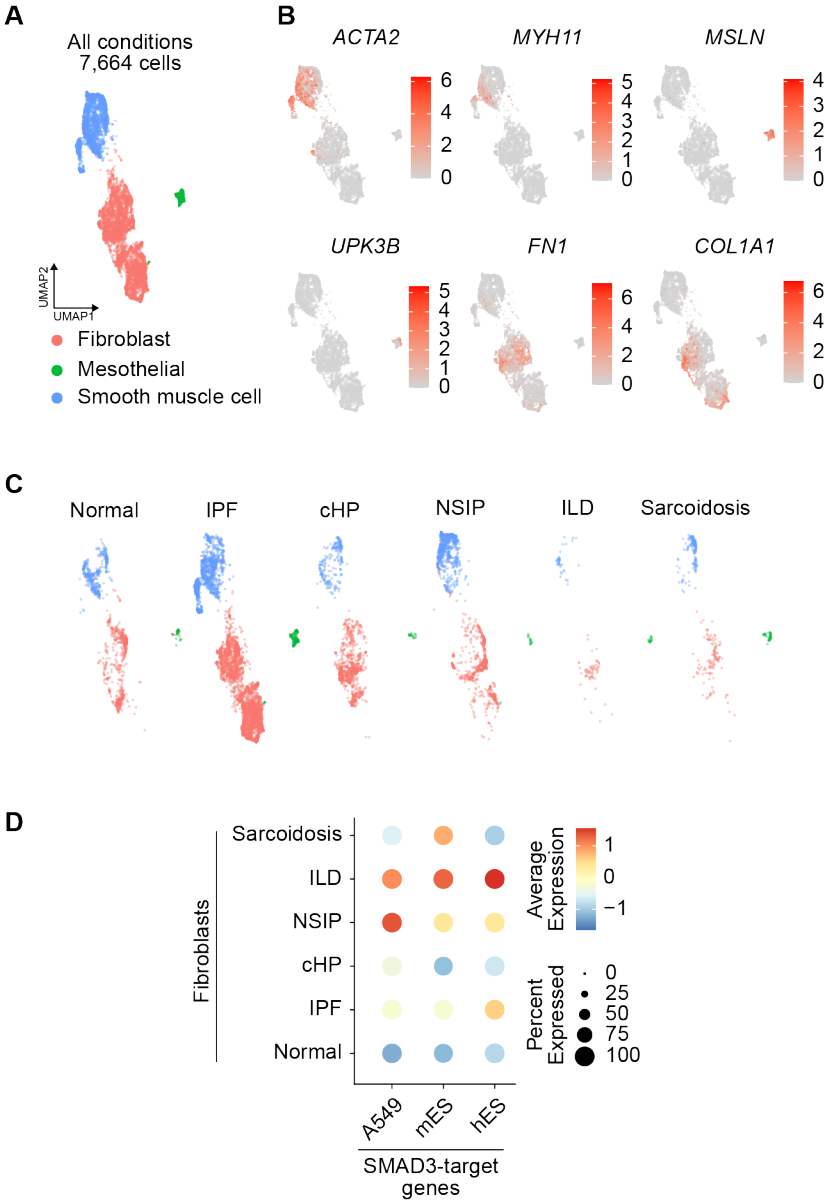


**Fig. S13. Elevated TGF-β signaling in lung fibroblasts of IPF patients.**
(**A**) UMAP showing the Mesenchymal compartment (*EPCAM*$^-$, *PTPRC*$^-$, and *PECAM*$^-$ cells) from the human scRNA-seq dataset (GSE135893; normal, IPF, cHP, NSIP, ILD, and Sarcoidosis). (**B**) Feature plots of indicated marker genes. *ACTA2* and *MYH11* for smooth muscle cells; *MSLN* and *UPK3B* for mesothelial cells; *FN1* and *COL1A1* for fibroblasts. (**C**) UMAP embedding displays cells colored by cell types split by each disease type. (**D**) Dot plots showing the expression of indicated genes and module scores of SMAD3-target gene sets in human lung fibroblasts.

## Fig. S14

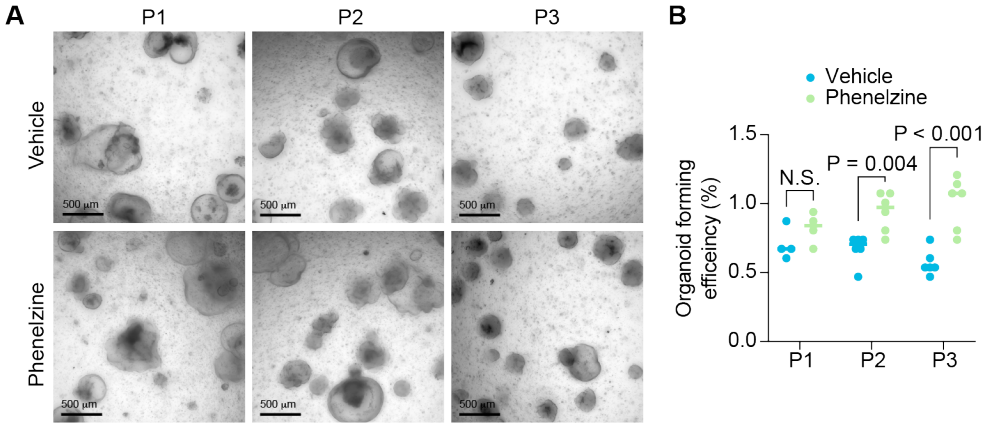


**Fig. S14. Phenelzine promotes LO formation.**

(**A**) Images of LOs with phenelzine (10 μM) at 12 days of indicated passage. (**B**) Quantification graph of lung OFE at 12 days of passage. Two-tailed Student's *t*-test; error bars: SD. The representative images are shown (n>=3).